Finding a clinical application for an ultrasound probe tracking system and proving its suitability

Validation of a robotic arm for 3D reconstruction of human anatomical features with ultrasound stitching

Master of Science Thesis

Vladislava Vladimirova Dinkova

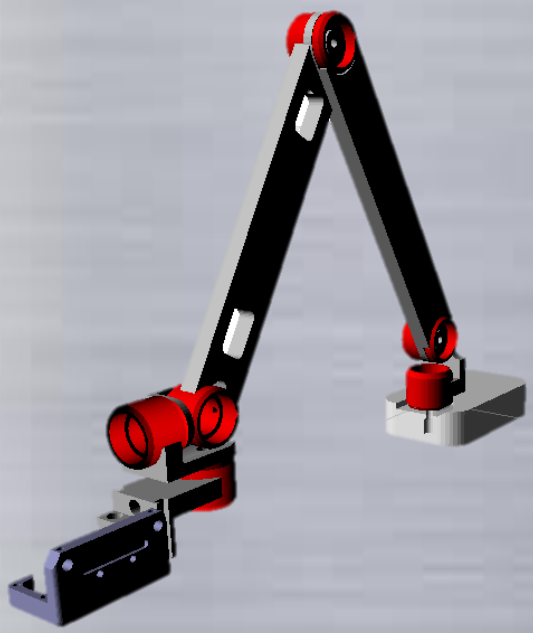

PHILIPS TU Delft

Finding an application for an ultrasound probe tracking system and proving its suitability

Validation of a robotic arm for 3D reconstruction of human anatomical features with ultrasound stitching

Vladislava Vladimirova Dinkova

To obtain the degree of Master of Science

at Delft University of Technology

25th of September 2020

Student number: 4935098

Thesis committee: Dr. ir. N. de Jong , TU Delft, supervisor

Dr. ir. F. van Heesch, Philips Research, supervisor

Dr. ir. A. Kolen, Philips Research, supervisor

Dr. ir. M.A.P. Pertijs, TU Delft

Dr. ir. V. Daeichin, TU Delft

Acknowledgments

This document is the end result of my master thesis at Philips Research and in collaboration with TU Delft. Completing the work has been slightly complicated by the unexpected, and sometimes still unbelievable, pandemic situation due to the corona virus.

I would like to thank Prof. Nico de Jong for his guidance during this work and his valuable feedback during our progress meetings.

During my thesis, I was extremely fortunate to have Frank van Heesch and Alex Kolen as my daily supervisors. I cannot thank them enough for all the brilliant discussions that we had, the constructive feedback that I received and all the support that I felt. They were the ideal supervisors that I could think about.

Thanks to the clinical experts that helped me in understanding what would be possible to provide with our technology in different clinical areas. In special, thanks to Babic Drazenko for your brilliant ideas and visionary insights. Also, thanks to Geert Gijsbers for his clinical vision and for offering me this exciting work for my master thesis.

I would like to thank the people from the In-Body Systems department for their warm reception in their group. Also, I am very grateful for the two very good friends that I made there, Claudio and Marco. Thanks for all the enjoyable moments together.

I am also deeply appreciative to my friends which supported during all this work, encouraged me and made me feel loved. I am very lucky to have you in my life. Special, thanks to Suryansh for being a sunflower in my life, always bringing hope and support, and for dedicating that much time in helping me. Thanks to Laura and Bozhidar for your immense support during the tough times, always make me cheer and share time with me online during the lockdown, without you everything was going to be much more difficult.

Last but certainly not least, I am blessed to have a very loving and supportive family to which I will be forever indebted. Thank you for believing always in me, supporting me in all my journeys and being pillars of strength in my life.

Vladislava Vladimirova Dinkova

14th of September 2020

Table of Contents

List of Figures

List of Tables

Summary

Ultrasound imaging is a widely available and highly portable real-time, ionizing radiation-free imaging modality used as first-line in multiple areas. Conventionally, its use is focused on providing 2D imaging using ultrasound probes. However, with the introduction of matrix probes, the acquisition of 3D scans became possible enabling the sonographer to accurately interpret the scanned anatomy without needing to build a possibly error prone 3D mental map and thus, decreasing operator-dependency. Although with this 3D imaging, volume estimation accuracy increases and surveillance becomes less difficult, matrix probes are expensive, have a limited field-of-view and produce a low contrast image. This necessitates the sonographer to still build a mental map whenever a portion of an anatomy is not fully visible in a single volumetric scan, leading to more laborious surveillance. Ultrasound stitching is investigated as a potential method to overcome these limitations by tracking multiple ultrasound scans and merging them using their position and orientation coordinates. To this end, this work uses a robotic arm as the selected tracking system for the stitching of 2D xplane ultrasound images. First, the initial clinical application for the system was derived using a combination of literature study and interviews with medical experts which led to the decision of utilizing the robotic arm for liver imaging and biopsy needle guidance.

The suitability of this application was validated with the evaluation of the three required stages namely anatomy reconstruction, needle path planning and needle insertion. Two phantoms mimicking lesions and surrounding vessels were fabricated for this purpose. They were firstly reconstructed by manually segmenting the elements of interest from multiple scans, placing these segmented scans in their respective 3D positions and finally applying an alpha-shapes reconstruction algorithm. Although the resulting reconstructed lesions showed volume overestimation in almost all evaluated cases, the 3D coordinates of the lesions' centroid could be estimated with a repeatability of less than 1 mm across repeated phantom scans for 72% of centroid coordinates in 3D space. By strategically selecting the position of scans to segment, it was possible to faithfully estimate the lesions' centroid by only segmenting four scans per lesion. The results were compared to the empirical approach obtained by segmenting a high number of scans per lesion and considered being closer to the ground truth. A difference smaller than 1 mm was observed for 60% of the centroid coordinates and a maximum difference of 4 mm was observed for one of the lesions' centroid coordinates. For the anatomy reconstruction stage, it was important to estimate the lesions' centroid since these dictated the biopsy needle direction. Once that was achieved and together with the position information about the surface of the phantom obtained with the robotic arm, it was possible to evaluate all the paths that connect the surface with the centroid and subsequently select only the ones that did not pass next to a vessel within a specific distance. This needle path planning also enabled the determination of the shortest needle path that causes the least tissue puncture. Finally and as an extension of using the robotic arm to track the ultrasound probe, the combined tracking of the probe with a needle holder was investigated for the needle insertion stage. The needle holder was used to maintain the needle always in plane with the ultrasound beam and it was placed at a preset distance with respect to the probe. The holder also provided insertion depth information that facilitated the representation of the needle via a line in the visualization environment whose end indicated the position of the needle tip. This position was updated in real-time with the information received from the needle holder while the needle was being inserted. The position of the needle tip was verified by overlapping real-time ultrasound images with the visualized line. Ultimately, to further illustrate the suitability of the robotic arm in a clinical setting, an ex-vivo and a clinical experiment for vessel tracking and reconstruction was performed.

1. Introduction

Medical imaging plays a crucial role in the diagnosis, preoperative treatment planning and posterior follow up of the patient. The quality of medical care has experienced a significant improvement with the introduction of advanced imaging technologies. Those technologies enable accurate diagnoses and precise treatment plans that improve patient outcome. The different imaging modalities can be in first place divided into anatomical imaging modalities, which image internal anatomical structures, and functional imaging modalities, which provide information of a particular physiological function [1].

1.1 Motivation

This Master Thesis is focused on ultrasound (US) imaging. US imaging, together with projection radiography, computed tomography (CT) and magnetic resonance imaging (MRI), is an anatomical imaging modality. An introductory overview of their working principle is presented in Section 1.1.1, followed in Section 1.1.2 by a description of why the improvement of the ultrasound imaging capabilities is a clinical need.

1.1.1 Existing methods

Projection radiography. This modality is called a projection because it represents the projection of a 3-D object into a 2-D plane. Into this modality, an x-ray pulse with an almost uniform cone beam shape is originated by an x-ray tube. The pulse passes through the body and is attenuated by the interactions with the different tissues, resulting in an exciting beam with a not uniform intensity profile. Then, a scintillator is used to reveal the intensity distribution by converting the x-rays in visible light. Finally, a photographic film, a solid-state detector or a camera is used to capture the light in the scintillator [1].

Computed Tomography. It is modality based on the attenuation of the x-rays when they propagate through the body. The difference with projection radiography is that in CT, the x-ray source is moved around the body. Multiple projections are collected for the same tissues locations but now from different angles. A CT scan consists of multiple rows of detectors whose output signals reconstruct one or more cross-sections of the patient's anatomy. In this way, after reconstruction, it is possible to obtain a truly tomographic image [1].

Magnetic Resonance Imaging. In the human body, there is a vast number of hydrogen atoms and the spin of the protons in the nucleus tends to align with a strong magnetic field when this one is present, resulting in a net magnetization of the body. By selectively exciting some body regions, it is possible to make groups with magnetic spins point to a different direction than the magnetic field direction. When they return to the position on which they are aligned with the magnetic field, they wobble (a movement called precession). Since they are charged particles, this precession movement generates a radiofrequency signature that can be detected with an antenna [1].

Ultrasound Imaging. This modality relies on the reflection of acoustic waves to create the images. In US imaging, the high-frequency sound is transmitted into the body and the returning echoes from body structures are received. Repetitive bursts of ultrasound (pulses) are generated. When the speed of sound in the media and the time-of-return of the pulses is known, it is possible to calculate the depth at which the reflector is. Furthermore, the intensity of the reflected pulses gives information about the strength of a reflector [1].

1.1.2 Clinical need

The above mentioned anatomical imaging modalities have their advantages and disadvantages which have to be taken into account when deciding which one to use for each patient case. The main disadvantages of projection radiography are that provides basic anatomical information for few tissue densities and it is an 3D volume projected into a 2D plane. Since the focus of this thesis is to provide a 3D image, this imaging modality is not going to be further discussed. The advantages and disadvantages of the other three imaging modalities are summarized in Table 1.

Table 1. Advantages and disadvantages of CT, MRI and US [2].

Imaging modality	Advantages	Disadvantages
CT	• 3D • Good spatial resolution • Good contrast resolution • Reproducibility • Shorter scanning time than MRI • Wide field of view	• Ionizing radiation damaging to the patient • Intermediate cost • Intermediate availability • No real-time
MRI	• 3D • Excellent spatial resolution • Excellent contrast resolution • Free of ionizing radiation • Reproducibility • Wide field of view	• High cost • Limited availability • Long scanning time • No real-time • Contraindicated for patients with ferromagnetic implants

US	• 2D/3D • Real-time • Free of ionizing radiation • Portable • Available to a large extent • Low cost • Can be used intra procedurally	• Operator-dependent • Lower contrast and spatial resolution • Limited field of view • Poor penetration through bone and air

The purpose of this project is to provide a 3D image because 3D images permit a better volume estimation of structures, the sonographer does not have to rely only on his mental map reconstruction to make a diagnosis and a treatment plan, and surveillance is less difficult. Table 1 has illustrated some of the advantages of US imaging. For example, it is a radiation-free imaging modality, in contrast to CT, which is highly important in order to avoid the appearance of secondary effects. Furthermore, it can be made more widely available because it is better portable and cheaper than CT and MRI. It is a real-time imaging modality which is essential during interventions (such as biopsies) since it can be used intra procedurally. Additionally, the scanning time is shorter compared to MRI, avoiding the formation of long waiting lists. These properties make US imaging the first-line imaging modality in many areas.

The use of ultrasound imaging could be extended even more if some of its limitations and disadvantages are solved. 3D matrix probes have been introduced into the market, which use electronic scanning to acquire 3D information. These probes have a 2D array of transducers that emit a diverging beam with a pyramidal shape enabling the acquisition of volumetric scans [3]. This has the advantage that the operator dependency is decreased since the sonographer does not have to elaborate a 3D mental map from stitching 2D slices and surveillance becomes easier due to an increase in repeatability [4]. However, the main drawbacks of the ultrasound matrix probes are the low image contrast and the limited field of view (FOV) [5]. As a result, in many cases it is not possible to visualize in only one volume the whole structure of interest and the sonographer still needs to create a mental map of the anatomy for diagnostic purposes. Furthermore, the low image contrast makes difficult the visualization of some structures and an accurate edge estimation [5].

Sophisticated tracking techniques exist in order to create 3D ultrasound scans that could overcome the limited FOV and low contrast image disadvantages of the ultrasound matrix probes. Those techniques involve the use of mechanical localizers, mechanical 3D probes and freehand scanners. Due to the focus of this thesis, only the last ones are going to be explained in the next section and these can be divided into ultrasound probe tracking systems (Section 1.2.1) and image-based techniques (Section 1.2.2).

1.2 Position tracking techniques to overcome some of the ultrasound limitations

Knowing the 3D position in space of multiple US scans adds ease of use since these scans can be stitched together. This tracking of the scans can be done by externally tracking the probe (Section 1.2.1) or directly from the image data itself (Section 1.2.2).

1.2.1 Ultrasound probe tracking systems

Ultrasound probe tracking systems provide the position and orientation coordinates of multiple US scans with the use of a sensor attached to the probe. As such, multiple scans can be correctly placed and combined in a 3D space. Electromagnetic tracking systems, optical tracking systems and passive encoded mechanical systems are the three main used ultrasound probe tracking systems.

Optical tracking systems. Active or passive targets are placed on the probe and are typically tracked with at least two cameras. By observing the targets from two different images and knowing their relative positions on the probe, it is then possible to calculate through triangulation the position at which the ultrasound scans were acquired [3]. Passive markers are retro-reflective spheres which are illuminated and appear as bright points in the cameras images. Active markers are light sources that are in the cameras view and they appear as even brighter spots in the cameras images. Optical systems can be highly accurate but their issue is the requirement for a line-of-sight between the targets and the camera [3][6].

Electromagnetic tracking systems. In this case, a number of small inductive coils, receivers, are placed on the probe and near to the patient there is a time-varying magnetic field generator. A system control unit activates the coils present in the field generator and monitors the data obtained from the receivers. These systems are relatively small and do not have the line of sight limitation as optical tracking systems do. However, their tracking accuracy can be affected by the interference with metallic objects, leading to distortion [6].

Passive encoded mechanical systems. In these systems, the US probe is attached to an articulated arm. This arm presents multiple movable joints on which encoders are placed and provide the angulation of each joint. This information, together with the known length of the links, is enough to obtain the position and orientation in 3D space of the attached probe by applying forward kinematics. A disadvantage is that many times these systems have a limited reach because the links should be as short as possible to improve their precision [3]. In addition, the physical arm connected to the probe might obstruct other instruments used during the procedure, such as biopsy needles in biopsy procedures [3].

1.2.2 Image registration based techniques

In the image-based sensing approach, the position and the orientation coordinates of the US scans are obtained by analyzing image features, instead of using position sensors. The features that are usually tracked are speckles and the analysis is based on speckle decorrelation [3]. The obtained images are divided into small sub-regions and the calculated decorrelations values are used to quantify how to place consecutive scans [3]. The biggest advantage is that no additional sensors need to be attached to the ultrasound probe. However, a disadvantage of these techniques is that the scanning should consist in moving the US probe in a rotational or linear manner at a constant speed to guaranty a large overlap between consecutive scans, decreasing the freedom of the sonographer while performing a scan. Furthermore, the accuracy of the image registration is limited by the signal-to-noise ratio and the low spatial registration [3][4]. The features in the ultrasound image to track are not very well defined causing many difficulties in the volume reconstruction.

1.3 Research Scope

The preceding sections have introduced the clinical need of a system that achieves ultrasound stitching and the state-of-art techniques investigated in order to achieve that. The selected technique for this master thesis is a robotic arm that has shown to be capable of achieving accurate positioning. This is a non-actuated robotic arm that is used as a sensing device and provides the position and orientation coordinates of multiple acquired US scans.

The main research question is to find a clinical application for the robotic arm tracking system at hand. It has to be an application where the currently encountered problems cannot be solved with another imaging modality or that the used imaging modality presents some disadvantage. Furthermore, the application should present a good market size.

After an extensive process involving a literature research and talks with clinical experts, the first main research question has been solved. Liver imaging for focal lesions detection and biopsy guidance is chosen as the first application. The liver is a very suitable organ to be imaged by ultrasound and it is not subjected to internal motion as the heart is. The organ is large, hence a single ultrasound volume does not cover the entire field of interest. The clinical need for liver scanning is large enough to investigate industrial solutions. In addition, biopsy guidance is chosen due to the intra-procedural character of ultrasound imaging and proper image guidance is not well established.

The next step in this research is to prove that the robotic arm is a suitable US probe tracking system for needle guidance during liver biopsy procedures. In order to demonstrate that suitability, multiple sub-questions have been addressed.

- Firstly, it was evaluated how accurately lesions can be segmented for their volume and centroid estimation.
- Secondly, it was studied if neighbouring structures can also be visualized for the planning of the biopsy and the selection for the best needle pathway.
- Thirdly, it was investigated the possibility to visualize in real-time the biopsy needle during its insertion path with a quality that has clinical relevance.

These three sub-questions have been answered by developing phantoms that mimic lesions with surrounding vessels. Finally, an ex-vivo and clinical experiment is carried out to observe the performance in a more realistic scenario.

1.4 Thesis outline

This master thesis has the following structure. Chapter 2 presents the clinical applications that have been considered as the first application for the robotic arm tracking system. A literature study was performed to understand the needs in different clinical areas, how ultrasound stitching could solve some of the current limitations and the reported performance of different already studied stitching techniques. Chapter 3 describes the research methods applied in the different stages. These stages were performed to give an answer to the sub-questions addressed in the previous Section. Chapter 4 starts with a detailed description of the logical and decision-making process behind the selection of the most suitable and valuable clinical application of the system. Next, the results of the different research parts are presented. In Chapter 5, the results are discussed, recommendations for future studies are described and the clinical relevance of the thesis is highlighted. Finally, conclusions are drawn in Chapter 6.

2. Literature review of clinical applications

Part of this master thesis focus was to find suitable medical applications for the robotic arm tracking system and select the most suitable first application to pilot the performance of the system. Therefore, this phase was backed with an extensive and systematic literature research and interviews with experts. The result is an understanding of the medical diagnostics and procedures that are performed with ultrasound and the areas where it would be possible to provide improvements in terms of accuracy, image quality, FOV and surveillance. Furthermore, a general understanding of limitations or problems that previous research faced when trying to achieve ultrasound stitching was gained.

The papers for this literature review were selected from Web of Science, Embase, Cochrane and Pubmed. Search key words such as “tomographic ultrasound”, “ultrasound stitching” and “multi-perspective ultrasound” were used. The abstract of the papers whose title indicated an affinity with the topic of this work was screened and the paper was fully read if a concordance from the abstract was perceived. Furthermore, additional information was obtained from meetings with researches who have worked in some of the position tracking techniques mentioned in Section 1.2, physicians and clinical scientists.

This chapter starts in Section 2.1 with a description of possible applications for vascular imaging. These applications include aortic artery imaging, carotid artery imaging and imaging for peripheral arterial disease, autologous bypass graft and arterio-venous (AV) fistula purposes. Sections 2.2 to 2.5 explore the possibility of using US stitching for cardiac, liver, thyroid glands and musculoskeletal imaging, respectively. Finally, Section 2.6 shortly illustrates the applications that were discarded from the beginning and why.

The applications described in this Chapter were evaluated in terms of the degree of improvement that could be provided with the robotic arm in comparison with the other tracking techniques. Furthermore, applications which suitability and feasibility could be proven with a phantom were selected due to the time limitation of the master thesis compared to the time needed for approval from an Ethical

Committee. Finally, also the size of the market was considered during the decision-making process. This process is described in details in Section 4.1 of the Results chapter.

2.1 Vascular imaging

2.1.1 Aortic artery

A life-threatening condition involving the aortic artery is an abdominal aortic aneurysm (AAA) [7]. An AAA is a local dilation of the abdominal aorta caused by a weakening in the arterial wall [8, pp. 121-138]. The major associated risk is a hemorrhage due rupture which could also lead to death [8, pp. 121-138]. Studies show that 80% of the patients that suffer an AAA rupture outside of the hospital and 50% of the patients that achieve to reach the emergency room died [8, pp.121-138]. The current protocol suggests that a surgical intervention has to be done when the diameter of the AAA if bigger than 5.5 cm in case of men and 5.0 cm in case of women or when there is a growth of the aneurysm equal or bigger than 1 cm per year [5]. However, some aneurysms rupture before they reach this threshold while others remain stable until a diameter of 8 to 9 cm [9]. Hence, it is required a more personalized rupture risk assessment that takes into account not only the diameter of the aneurysm but also other parameters in order to prevent premature rupture or overtreatment [5].

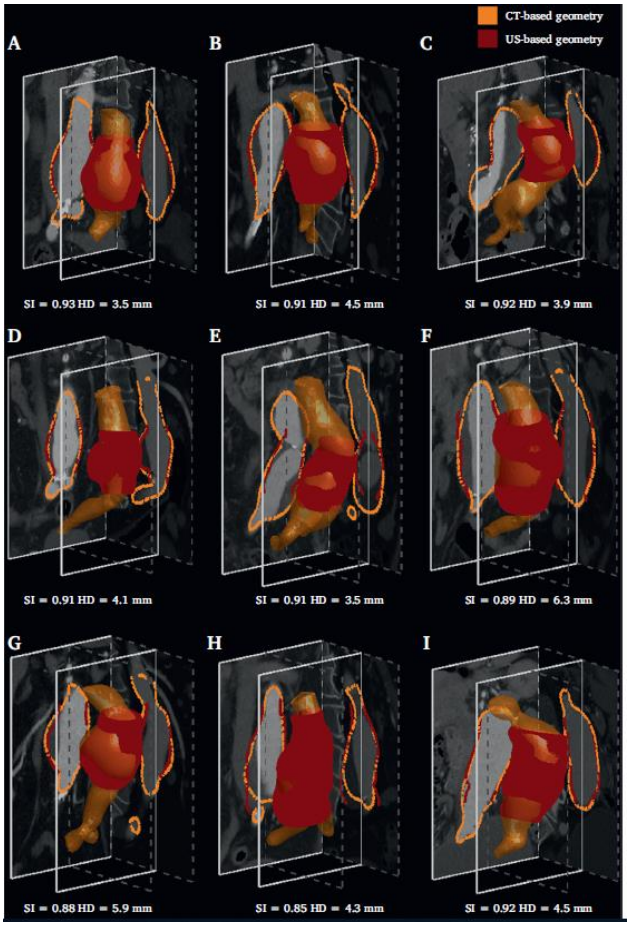

Figure 1. Nine AAA obtained from a CT scan (orange contours) and from an automatic segmentation algorithm applied over 3D US scans (red). Subfigures A-E represent the results from a single 3D scans while subfigures F-I represents the results of multiple 3D fused US scans [5].

Explained from a biomechanical perspective, a rupture of the aneurysm will occur when the local wall stress is higher than the wall strength [9]. Wall stress analysis is a method that has been proposed in order to achieve a more personalized risk assessment and it shows promising results [7]. It has been possible to predict in patients with a similar diameter of AAA if the aneurysm was going to rupture or not [7]. Through this method, peak wall stresses are calculated with patient specific aneurysm geometry and blood pressure [5]. The patient specific geometry is generally obtained with the use of CT or MRI [5]. Although recent studies have shown the feasibility of 3D ultrasound for the assessment of the geometry [5]. However, the limited FOV of 3D ultrasound is the main drawback for its use [5]. In one single 3D volume is not possible to capture large AAAs, including both shoulders, and that is the case of 40-45% of the patients [5]. A way to solve this limitation is the acquisition of multiple US scans with the use of a probe tracking system for their posterior stitching or applying image fusion algorithms for the same purpose [5]. Studies applying registration algorithms to multi-perspective US scans acquired from patients with AAAs show a good similarity between the

reconstructed aneurysm geometry derived from US and CT [5][9]. In one of the studies, the lumen-wall interface in the transverse cross-sectional plane was manually segmented from the data. The obtained average similarity index (SI) between the geometries reconstructed with US and CT was equal to 0.81 [9]. In general, SIs of 0.70 or higher indicate a good agreement between two geometries [9]. In the other study, 40 AAA patients participated [5]. For 20 of these patients, it was necessary to acquire a multi-perspective 3D US scan since it was not possible to capture their whole aneurysm in only one 3D ultrasound. In this case, a fully automatic segmentation algorithm of the aneurysm was applied, which yield an average SI of the reconstructed geometries with US and CT equal to 0.89 [5]. In Figure 1, some of these geometries together with their SI can be observed. Therefore, multi-perspective US and posterior image registration is a valid method for aneurysm reconstruction for its posteriori use for wall stress estimation.

The two treatment options for an AAA are an open surgery repairing the aneurysm with a tube graft or an endovascular aneurysm repair (EVAR) which is a less invasive option [8, pp. 121-138]. Sometimes, during an EVAR operation, the stent graft is unable to exclude the aneurysm sac from the circulation, leading to the formation of an endoleak and sac expansion. This requires a secondary intervention post-EVAR [8, pp. 121-138]. The usability of tomographic ultrasound for the detection of endoleaks is still not extensively studied. However, a study involving contrast-enhanced tomographic ultrasound (CEtUS) with the use of an electromagnetic tracking system shows that this a sensitive technique for the detection of type II endoleaks [8, pp. 121-138].

2.1.2 Carotid artery

The third leading cause of death in the world, behind ischemic heart disease and cancer, is stroke [10]. Thirty per cent of the ischemic strokes are caused by carotid disease [10]. The severity of the stenosis is considered as the principal indication for carotid endarterectomy (CEA) [10]. To provide the maximum benefit from the operation, this has to be done as soon as possible after symptoms of cerebral ischemia [10]. However, the percentage of stenosis is not the most reflective indicator for stroke prediction since patients with the same level of stenosis can be asymptomatic or symptomatic [8, pp. 139-153]. Furthermore, previous studies have suggested the possibility of outward remodeling of the arterial wall to maintain luminal diameter, reducing the degree of stenosis and showing that is an unreliable assessment criterion [8, pp. 139-153]. It is now suggested that carotid plaque volume (CPV) may be a better predictor for stroke than the degree of stenosis [8, pp. 139-153][10].

3D images facilitate not only the understanding of the morphology but also the calculation of carotid plaque volume since the plaque mass can be more accurately estimated than from 2D images [11]. Furthermore, 3D images increase the sensitivity with which to track plaque volume changes over time [11]. One research group decided to study in patients undergoing primary CEA the feasibility of using an electromagnetic tracking system together with a duplex US scanner for CPV estimations [10]. The results from some of the participants were omitted due to an intense acoustic shadowing that made interpretation of the fused scan impossible. The results from the remaining participants show a close correlation of CPV measured with the tomographic US and measured in the endarterectomy specimen with minimal bias [10]. These results illustrate the suitability of using tomographic US for CPV estimation.

Another research group used also an electromagnetic tracking system to establish if the best results for CPV are obtained with B-mode tomographic US, CEtUS or fused tomographic US by comparing the estimated volumes through these methods with the ones of the endarterectomy specimens [8, pp. 139-153]. The results from some of the participants were again excluded due to an excessive acoustic

shadowing. By a slight difference, the best results were obtained from the reconstruction using CEtUS. Their research showed that tomographic US is a method to measure with high precision and minimal bias CPV. They also indicated the need of stablishing a clinical protocol that defines the starting and ending point used for measuring CPV.

Furthermore, it has been found that US measurements of carotid plaque area and height are predictors of coronary artery disease (CAD) [12][13][14]. The current clinical standard for the diagnosis of CAD is coronary angiography. However, its application is not recommended for initial screening since it is invasive and costly. Thus, carotid plaque assessment could be used as an initial risk screening tool although it has not been already implemented as a vascular biomarker [14]. 3D US has been found to be more strongly predictive of CAD than 2D US [12]. This is due to the fact that plaque has an irregular shape and if 2D scans are out of plane, they may miss the real extend of the plaque while 3D allows imaging the plaque in all the planes [12].

2.1.3 Peripheral artery disease

Atherosclerosis is frequently observed in lower limb arteries causing peripheral arterial diseases (PAD). The severity of the PAD is evaluated based on the degree of stenosis and its location [15]. If the case is severe, a catheter angioplasty with or without stenting may be recommended to avoid limb loss and improve the patient's quality of life [8, pp. 154-167]. For the initial assessment of PAD, duplex US is often used. However, its accuracy is moderate for the diagnostics of crural artery disease and it is limited used for the assessment of arch, pedal and digital arteries. Thus, in case of possible PAD in the crural or pedal arteries, vascular scientists reply on the use of angiographic imaging modalities such as computed tomographic angiography. Besides the radiation dose received, also nephrotoxic contrast is applied in this case, which is not suitable for patients with kidney diseases [8, pp. 154-167]. Contrast-Enhanced Ultrasound (CEUS) has been reported to provide superior results for the assessment of below knee arterial diseases.

[8, pp. 154-167] evaluated the feasibility of using CEtUS for the assessment of pedal and crural artery diseases. They used an electromagnetic tracking system and the study was performed in a clinical setting. In addition to the CEtUS, the patients underwent a clinical angiogram for comparison and the angiography was assumed to be the gold standard. The agreement between the gold standard and CEtUS was moderate since in some instances severe stenosis or occlusion was observed with in angiograms but not in the tomographic US scans and in other cases, severe stenosis or occlusion was observed with CEtUS but not with angiography [8, pp. 154-167].

Furthermore, [15] performed a study where they used a 6 DOF robotic arm as an US probe tracking system. In their case, it was possible to "teach" the arm a scanning path and later the arm was able to reproduce that path with controlled speed. Since the scanned volume was regularly sampled, they assumed this approach to provide a higher reconstruction accuracy than a 3D freehand system where some parts could be less accurate reconstructed due to a fast scanning and less data available. The system was tested with a vascular phantom with double stenosis immersed in a water bath. A sketch of the phantom and its reconstruction can be seen in Figure 2. The exact area reduction in the physical phantom was known for both stenosis and thus, a comparison between those values and the ones obtained from the reconstructed 3D phantom was possible. The errors were always between 2.2 % for both stenosis.

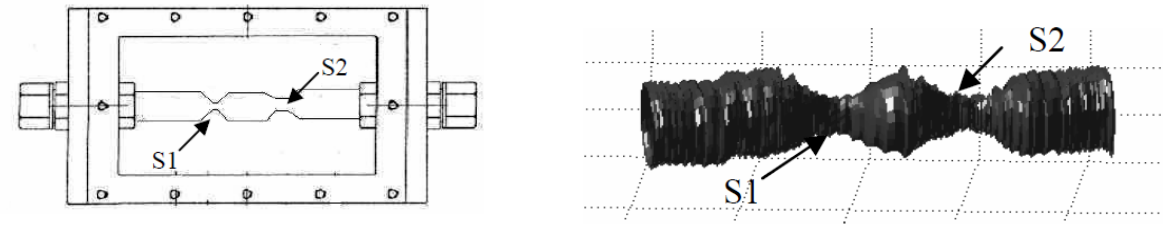

Figure 2. A sketch of the phantom used (left) and the resulted reconstruction (right) [15].

2.1.4 Autologous bypass graft

In severe coronary heart diseases with significant cardiac ischemia, it is recommended to perform a coronary artery bypass grafting (CABG) in order to restore sufficient blood supply to the myocardium. In addition, some patients with severe PAD may also require a bypass surgery, instead of a catheter angioplasty [8, pp. 168-182]. Using duplex US before these procedures for vein mapping is essential, showing a good correlation with surgical measurements and it clearly demonstrates if a vein is or is not appropriate for harvesting a conduit. If the vein presents abnormalities, such as areas of varicosity, is unsuitable for being used as a bypass graft [8, pp. 168-182]. However, duplex US provides a dynamic assessment and it requires that the vascular scientists build a 3D mental map of the vascular pathology and vessel's anatomy. As a result, there should be a high level of trust between the vascular sonographer and the surgeon for the selection of the optimum vessel. This trust-based procedure could be improved with the use of tomographic US since operator dependency is minimum. It is less error prone to identify the optimum bypass graft in 3D images than in a written duplex US report [8, pp. 168-182].

[8, pp. 168-182] used an electromagnetic tracking system for tracking in 3D space multiple duplex US images and merge them. In the study participated patients undergoing a peripheral bypass or CABG. Pre-operative images were acquired by a vascular scientist with duplex US and tomographic US. Before the operation, the surgeons only received the standard duplex report, following the clinical standard, and in order to not influence their decision. After the operation, they could see the duplex report again and they could also see the tomographic US images. The findings from the harvested autologous conduits when comparing both modalities revealed the following results. Tomographic US was preferred in more instances than duplex US when surgeons were asked about which modality was more valuable in deciding which vessel to harvest, which modality provided something to help them in deciding which vessel to harvest and which modality had a better agreement with the intraoperative findings. Finally, in more than half of the cases, surgeons agreed that tomographic US could have replaced duplex US [8, pp. 168-182]. These results show potential use of tomographic US for autologous bypass grafts.

2.1.5 AV fistula

An AV fistula is created when a vein and an artery are joined together under the skin. This creates an increase in the blood flow in the vein since the blood pressure in the artery is higher than the blood pressure in the vein and when they are joined, some of the arterial pressure is transferred to the vein. The increase in blood flow makes the vein suitable for hemodialysis. Aneurysmal changes and flow-limiting stenosis are thought to appear when turbulence in the blood flow creates high shear stress, which leads to intimal damage. If this stenosis is not detected and treated it can lead to thrombosis of the AVF, which is the largest cause of morbidity in patients with hemodialysis. For surveillance of the AVF, duplex US is usually used and when there is a diameter reduction greater than 50%, an angioplasty is

recommended. However, clinicians often cannot correctly interpret the anatomy of the AVF as a skilled sonographer. This is due to a lack in experience and practice in building a mental 3D map of the anatomy and it leads in many cases to misdiagnosis. Thus, there is a need to decrease operator-dependency in interpreting the images [8, pp. 183-194].

In [8, pp. 183-194], they used an electromagnetic tracking system to provide tomographic US results from patients with AVFs. They compared against fistulography the results obtained with the tomographic US and the ones obtained with duplex US in order to identify and estimate flow-limiting stenosis. They did not observe any meaningful difference between the results reported with tomographic US and duplex US when compared to fistulography. However, less imaging time and less skills were needed to assess the AVFs when tomographic US was used [8, pp. 183-194].

2.2 Cardiac imaging

Echocardiography consists in acquiring cardiac images with the use of US to assess the structure and function of the heart chambers, valves, pericardium and proximal vessels supplying the heart with blood. Transthoracic echocardiography (TTE) is the most common practice where images are obtained from three main echo windows – parasternal, apical and subcostal window [16]. In echocardiographic procedures contrast can be administered to the patient to improve image quality for left ventricular systolic assessment. Furthermore, stress echocardiogram for ischemia evaluation can be obtained by "stressing" the heart through exercise or dobutamine [16]. Echocardiographic evaluations can be performed with 2D or 3D US. In quantitative clinical measurements, 3D US presents a clear advantage over 2D US since no geometric assumptions about the cardiac chamber have to be made. This leads to a higher reproducibility and accuracy in the estimation of the left ventricular volume and ejection fraction, for example. However, only a minority of patients having a TTE can benefit from this advantage due to the limited FOV of 3D US probes that makes impossible to view in some cases the whole heart anatomy in one scan. Furthermore, these probes present low signal-to-noise ratio and low spatial resolution [4]. Echocardiography fusion of multiple scans can improve the FOV limitation and until some extend, it can also improve the aforementioned other two limitations. This improvement would be fundamental in stress echocardiography where it could be easier to track the same view in the different stages of the test and decrease the required training [17][18].

[4] investigated the feasibility of multi-view fusion echocardiography using an optical tracking system. The study was performed in a phantom and a patient with the fusion of 3D US scans. They tracked both, probe movement and phantom/patient movement by placing markers on the probe and the phantom's surface/patient's skin. ECG data was also obtained to fuse the scans based on R-R wave peaks. The patient was asked to hold his breath during acquisition. During the experiment, the phantom and the patient were moved to different positions, in order to demonstrate that with the surface/skin markers, it is possible to compensate for movement, and the probe was placed at different orientations. Their results proved that this approach can be used to compensate for significant patient movement, that it is possible to obtain an image where the boundaries of the myocardium will be continuous and that this technique does not involve stitching artifacts. [19] also investigated the use of skin markers and probe markers together with an optical tracking system in order to achieve stitching of 3D echocardiographic images. However, they did not move the patients but focused on better improving the movement compensation in between multiple breath-holds by only fusing data sets from the same breath-hold position. They showed that ignoring this compensation can lead to inaccurate alignment of multiple scans as it can be seen in Figure 3 since the breath-hold positions can differ significantly. They obtained an improvement of the FOV and an increase in SNR.

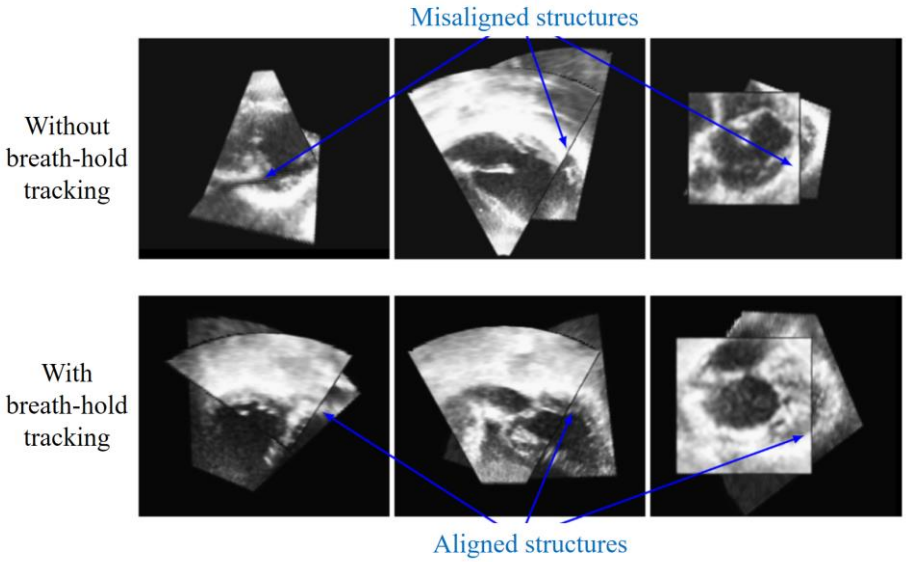

Figure 3. Illustration of the importance of breath-holding compensation for echocardiography fusion [19]. In the first row it is possible to see the result when no breath-holding tracking is applied and in row two when breath-tacking is applied.

The use of an electromagnetic tracking system was studied by [20]. They used a dynamic heart phantom for this purpose, which also provided ECG information. After the alignment of multiple 3D US scans, the resulting image was near to an optimal alignment but further improvements were necessary due to errors in the tracking data [20]. Lastly, [21] used a commercially available passive robotic arm as a probe tracking system. They performed their experiments in a heart phantom and by fusing nine 3D US scans they observed an improvement of 98.5% in the FOV with good alignment quality [21]. The results after the fusion of two scans (column 1 and 2) in three cases can be seen in column 3 of Figure 4.

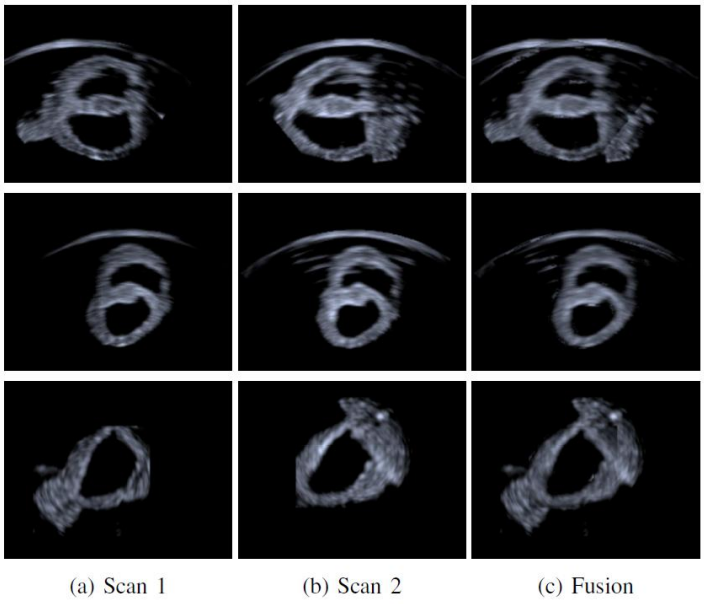

Figure 4. Example of the results when two 3D echocardiography scans are fused. In the first and second column are shown the scans used for the fusion and in the third column are shown the resulted fused image for three cases [21].

2.3 Liver imaging

The incidence of primary liver cancer is increasing in many developed countries and it is the third cancer-related cause of death worldwide [22]. Additionally, the liver is the most common solid organ where to develop metastatic cancer [22]. Currently, the usual approach for taking a biopsy of the liver is based on the acquisition of a preoperative CT scan, for tumor visualization and path planning, the use of 2D US for needle guidance and the acquisition of another CT scan, after insertion is completed, to confirm the accurate location of the needle [22]. The same approach is followed for the application of loco regional therapies using ablation probes. This protocol is a result of the significant radiation dose delivered by the CT scanner, making it unsuitable to use as an intraprocedural image-guidance modality [22]. However, the use of 2D US as intraprocedural modality requires the physician to build a mental 3D map of the anatomy of the patient. This step requires a lot of practice and experience, and it is crucial since a 3D image is needed in order to evaluate the extent and volume of the tumor, to be aware of the 3D position of neighboring structures, such as vessels or gallbladder, and to plan the intended insertion paths [22]. Thus, an ideal intraprocedural imaging modality for liver tumors should be fast enough to achieve real-time guidance, radiation dose free, adequate to the liver anatomy, capable to visualize in 3D space the tumor, the surrounding structures, and the biopsy needle or ablation probe [22]. Currently developed systems for 3D US image-guided intervention make use of probe tracking systems or 2D array transducers. The last ones do not solve all the problems due to their limited FOV. In liver imaging, an extended FOV is needed since it is a large organ, it presents a complex vasculature and a large portion underlines below the ribs [22]. Furthermore, it is needed an adaptable 3D scanning method by combining a narrow window for intercostal scanning with a wide FOV for subcostal scanning. By achieving that, a large FOV scan of the liver can be acquired which includes multiple anatomical landmarks such as surfaces and vessels branching which facilitate inter modality image fusion [22].

A method explored for liver imaging using US stitching consists of the use of an automated handheld assembly that moved accurately the US probe in a predefined path [22]. With that system, it was possible to move the probe with translational and/or tilting movements to a maximum linear extend of 3 cm and a maximum angle of 60°. By combining both types of motion, a larger FOV was covered. They acquired 2D US scans and since the trajectory was known they could place and stitch them in the 3D space [22]. They evaluate the volume measurement error with a tissue mimicking phantom with multiple lesions inside. The size of the lesions where such that they also fit in a 3D scan obtained with a matrix probe. Both measurements showed a great agreement in the volume estimation. The accuracy with which biopsy needles orientations and relative positions can be estimated from the reconstructed image was also assessed. For that, they introduced two needles into a tissue mimicking phantom with the help of templates that maintained known distances and angles between the needles. They compared the real distances and angles with the calculated from the reconstructed phantom using the automated handheld assembly and the ones calculated from a CT scan. The results from the CT scan were more accurate but the ones obtained from US stitching were also acceptable. A limitation that they observed in their study was the resolution of the scanner and the needle visibility, which makes challenging an accurate localization of the needles.

In another research [23], they used an electromagnetic tracking system for the exploration of abdominal organs (liver and kidneys). The aim was to compare conventional 2D US with tomographic US by evaluating through both methods organ size and in the case of the volunteers with lesions, the morphology and size of those lesions. Furthermore, the sonographers were asked to evaluate the image quality obtained through both methods. The ability to detect with the tomographic US focal organ lesions was satisfying in the case of patients with an outstanding image quality in conventional US. However, the diagnostic precision and image quality in the whole study was in average superior with conventional US compared to tomographic US. Metric assessment of the kidneys was satisfactory with a good agreement between both methods but it was not that satisfactory for the left liver lobe, where there were deviations between both methods. Furthermore, only 57 out of the 74 lesions diagnosed with conventional US were also diagnosed with tomographic US [23]. Figure 5 illustrates some of the obtained results with conventional 2D US and with tomographic US. Figures 5A and 5B present cases where the image quality of the tomographic US is good but Figure 5C shows a case with low image quality and where hyperechoic lesions cannot be identified. This shows that the system used in this study to achieve US stitching requires further technical improvements.

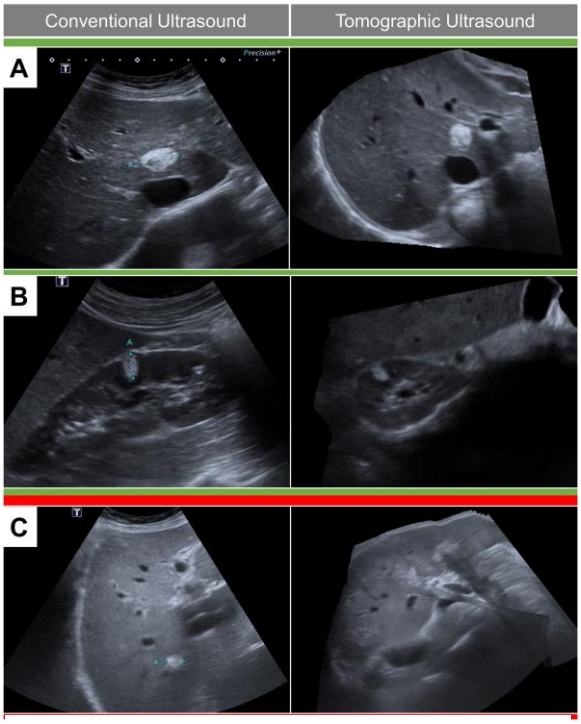

Figure 5. Comparison of US scans of abdominal organs obtained with 2D US and tomographic US. A) and B) presents results with good image quality in the reconstruction with tomographic US. C) presents a case with low quality [23].

2.4 Thyroid glands imaging

Thyroid gland is a butterfly shaped gland located on the front of the neck and it is one of the largest glands in the human body [24]. Its size and shape varies depending on factors such as age, gender, iodine availability, smoking habits and environmental factors [25]. Most of the thyroid diseases suppose a change in the size and shape of the gland. A correct estimation of its volume is highly relevant for the planning of the radiotherapy and the monitoring of the therapeutic effects [25]. Therefore, it is highly important to have a technique that allows surveillance of the state of the gland over time [24]. For the assessment of the thyroid's volume, ultrasound imaging is usually the modality of choice [24][25][26]. Advantages of using this modality are absence of radiation exposure, good anatomical resolution, good cost-effectiveness and good soft-tissue contrast [25][26]. Today's clinical standard for thyroid imaging uses 2D US and assumes that the gland has an ideal shape to which, a rotation ellipsoid model can be applied [25][26]. This assumption is reasonable for ordinary thyroid glands but in the case of diseased glands or glands with anatomical variations, this estimation can be highly error prone [25][26]. Furthermore, in the case of large volume thyroid glands with some deformations, intra- and inter-observer estimations may cause important volumetric errors [25][26]. 3D US is a possible method to overcome these limitations, which can also allow data storage of the volume datasets for its posterior analysis. Additionally, manual tracing can be used for volumetric analysis in 3D datasets. This method for the estimation of the thyroid's volume shows a high agreement with their actual size. However,

highly enlarged glands may not fit in one single 3D scan due to the limited FOV of common 3D US probes [25][26].

In [25], they studied the feasibility of stitching two 3D US volumes containing each one of them, a partial volume of the glands. They also assessed the accuracy of the estimated thyroid gland volume in the extended FOV US scan. For this purpose, they used water filled balloons of different volumes with a thyroid shape. The US probe was tracked with an electromagnetic tracking system and scans of the left and right lobes of the simulated glands were acquired separately with the inclusion of the isthmus [25]. The results of the volume estimation of the phantoms showed a high agreement with the real volume for all the shape and sizes of the phantoms [25]. An example of the reconstruction can be seen in Figure 6. The same research group performed another study using the same phantom but instead of using an electromagnetic tracking system, the investigated the use of mechanically swept convex and linear probes [26]. They found that the convex probe provided a good agreement in the volume estimation for all the sizes and shapes of the thyroid phantoms. However, with the use of a mechanically swept linear probe it was possible to estimate volumes only up to 50 ml [26]. Furthermore, in both studies, the manual tracing method provided superior results than the ellipsoidal model method, but it was also more time consuming [25][26]. On the other hand, [24] focused in the development of a semi-automatic segmentation algorithm from US scans using a modified active contour algorithm. The scans were acquired from patients and phantoms while the probe was tracked with the use of an electromagnetic tracking system. The algorithm requires that the user initializes the first mask for the starting of the active contour procedure. In the rest of scans, the initializing mask is automatically computed by the calculation of the center of mass of the preceding scan [24].

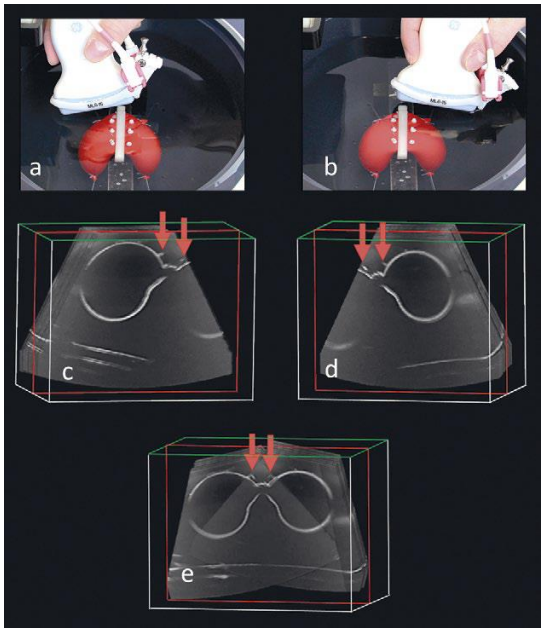

Figure 6. Reconstruction of thyroid gland phantom. A) and B) show the separate scanning of each lobe and in C) and D) it is possible to see the acquired data sets from each lobe. Finally, E) shows the reconstruction [25].

Obtaining an extended FOV scan of the thyroid can also be beneficial for the observation of all the possible nodules present in the gland and deciding which will be the best biopsy needle path in order to take a sample. US-guided fine-needle aspiration is the standard diagnostic modality for the evaluation of thyroid nodules [27]. It is a technique that presents high safety and diagnostic accuracy but its main drawback is the high rate of inconclusive results (approximately 22.4%) [27]. During a meeting with a physician [28] in order to explore the best application areas for the core system of this master thesis, he indicated the possible value of the system in obtaining thyroid biopsies. It is highly difficult to take a good sample of the thyroid nodules due to their small size. Usually, a physician needs multiple attempts to obtain a good biopsy sample [28]. This increases the discomfort of the patient, the time spent taking a biopsy and the number of samples to analyse [28].

2.5 Musculoskeletal imaging

The high reflectivity of US waves in bone makes US imaging a promising imaging modality for the investigation and evaluation of bone fracture. Disturbance of the smooth outline shape of the bone and

haematoma are indicators of fracture and are easily visible in US [29]. Previous studies for fracture repair monitoring with the use of 2D US have shown that with US it is possible to visualize the earliest stages of the healing process and that complication can be identified at its beginning stage [29]. Despite these advantages, 2D US has not been used to an extensive extent for fracture monitoring compared to X-ray. This poor penetration into the field is due to the high operator-dependency and the difficulty of obtaining the same view during surveillance of the fracture [29].

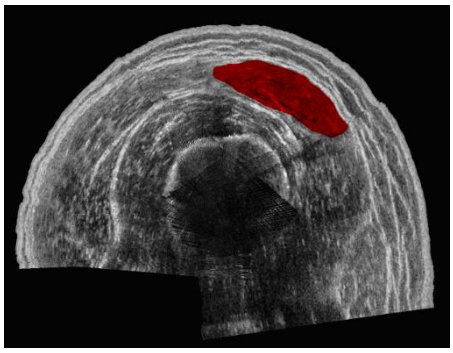

Figure 7. 3D US image obtained with an optical tracking system. The rectus femoris muscle is segmented in red [29].

Additionally, US can be used for muscle volume measurements. Changes in the muscle volume indicate injury, disuse or disease of the skeletal muscle. Furthermore, muscle volume could also be an indicator of progress and effectiveness of a rehabilitation program or treatment. They key of these studies is to accurately measure the muscle volume and that is limited when 2D US is used since approximations similar to the ones made in anthropometric measurements are assumed. 3D US imaging could provide more accurate muscle volume estimations and at the same time solve the limitations of operator-dependency and repeatability for fracture monitoring [29].

[29] decided to study the suitability of using an electromagnetic tracking system for the acquisition of 3D US scans for the purposes of monitoring fracture repair and estimating muscle volume. They achieved to obtained views of the patients anatomy that are impossible to acquire with 2D US but the probe positions provided by the tracking system showed a very low level of accuracy and reliability and thus, their method could not be used in a clinical setting. Therefore, they decided to perform another research using this time an optical tracking system. In this case, the results were satisfactory and they were able to properly identify the facture pattern and determine the area where the callus was forming. In 3 out of the 4 cases that they studied, the observed that signs of bone healing were earlier detected in 3D US than in X-ray. Furthermore, they also estimated muscle volume using and in Figure 7, it is illustrated the rectus femoris muscle segmented in red. The calculated volumes from the 3D US reconstruction differed within ±16% from the volumes estimated from MRI scans. The biggest factor influencing volume estimation was the difficulty in identifying muscle boundaries [29].

2.6 Excluded applications

Applications on which transvaginal or transrectal ultrasound is used were discarded since the range of movement is limited in them and the full potential of the robotic arm would not be explored. Obstetrics applications were also discarded since the fetus could move during the scanning from multiple perspectives and it is not possible to compensate for this movement, as it is possible with certain accuracy for the breathing and cardiac movement.

3. Methods

This chapter introduces the reader to the equipment, resources and algorithms used and developed throughout the experiment. Since the scope of the thesis is to find a clinical application for the robotic arm and prove its suitability, some of the initial equipment and algorithms have been developed at Philips Research before the start of the thesis. This is the case of the design and fabrication of the robotic arm itself, its model in the Robot Operating System (ROS) framework and the development of a socket between the US signal receiving PC and the ROS PC. The provided software by [30] to display images in the 3D visualization environment of ROS as 'textured quads' was also used to display the US scans in the visualization environment of ROS, RViz. Furthermore, the initial algorithm based on thresholding for displaying some of the features of these textured quads in the 3D space was developed at Philips Research before the start of the thesis, although it had to be adjusted to the needs of the final project. Additionally, the model of the robotic arm was improved during the internship of the author at Philips Research and the accuracy and repeatability of the arm were estimated during this period too.

The chapter starts in Section 3.1 with a description of the robotic arm and an explanation of the workflow of the equipment involved in achieving US stitching and biopsy needle guidance. In Section 3.2 the first method to evaluate the shape and size of a reconstructed object is described. In Section 3.3 the process of making the phantoms with lesions and surrounding vessels is detailed, together with the final reconstruction algorithm, the algorithm for the needle path planning and the setup and method used to illustrate the possibility of improving the needle visibility while approaching a lesion. Section 3.4 describes how vessels were reconstructed in an ex-vivo and clinical evaluation. Finally, Section 3.5 describes the developed algorithms to attempt to achieve an automatic or semi-automatic segmentation of the areas of interest.

3.1 Robotic arm as an ultrasound probe tracking system

3.1.1 Robotic arm description

A 6 degrees-of-freedom (DoF) robotic arm was designed and made at Philips Research using aluminium as a material. The arm consisted of seven parts, called links, assembled together, and at each assembling point, called joint, there was a magnetic rotatory encoder (RM08, RLS). In total, six of these 12-bit

resolution encoders were included in the arm and they provided absolute values for the orientation of each of the arm's joints, which were read in sequence. At the end of the arm, a link was included to anchor the US probe. This link, called probe holder, ensured a fixed position of the probe with respect to the arm end-point during scanning. An image of the arm can be seen in Figure 8A.

The main part of the software was developed in the ROS framework. ROS includes a set of software libraries and tools for building robot applications. In ROS, the folders on which you organize your software are called *packages*. Each *package* must contain a package.xml file, where the package's properties such as its name, authors, version number, dependencies, etc. are defined, and a CMakeLists.txt file, where it is described how the code should be built and installed. Additionally, inside of a *package* it is possible to have one or more *nodes*, which are the executables that contain the implemented algorithms. The type of data used in ROS is called *messages* and therefore, the algorithms developed in the *nodes* can *publish messages* to a *topic* or *subscribe* to a *topic* from another *node* to receive *messages*. These ROS specific terms are explained here since they will be further used in this report.

Linux Ubuntu was the selected operating system on which to use ROS since it provides much better support compared to Windows. ROS includes a python and a C++ library and codes in both programming languages were developed for this work. Although C++ was mostly used since the community using this programming language is bigger and more examples could be found.

The arm had a calibration block on which it could be placed as illustrated in Figure 8A. The configuration of the arm in this position was used to build a model of the arm in ROS, which constituted its Unified Robot Description Format (URDF) file. Since the arm was designed at Philips, it was possible to use the .stl files utilized for its fabrication for the generation of a highly realistic model, whose result can be seen in Figure 8B. As previously mentioned, the encoders of the arm were absolute and their values when the arm was standing in the calibration block were taken as their offset. Therefore, through forward kinematics it was possible to see the arm moving in real-time in the RViz visualization environment as it was been moved in real-life. Furthermore, it was possible to obtain the translation and rotation of every link of the arm with respect to another. This was achieved thanks to the transform (tf) package of ROS that provides a library with mathematical functions for kinematic routines to transform kinematic data from one reference frame to another.

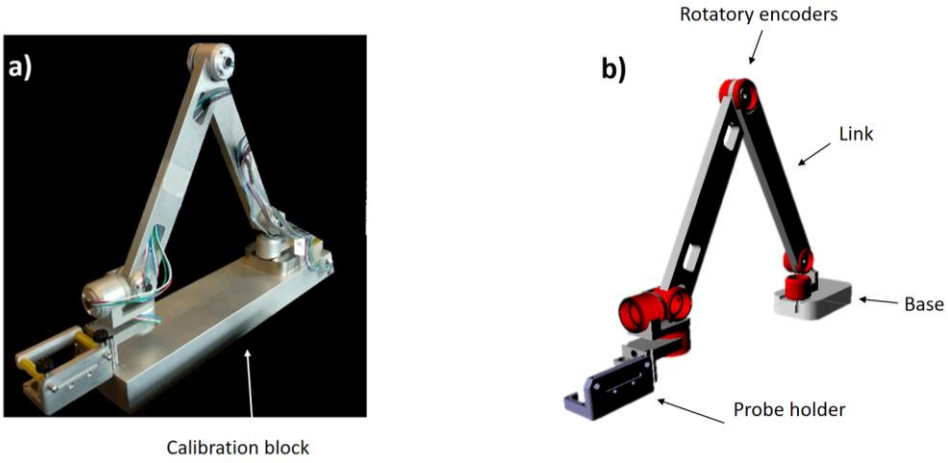

Figure 8. Robotic arm. A) Photo of the robotic arm. B) Image of the model of the robotic arm visualized in RViz.

The accuracy and repeatability of the arm was estimated with the use of a 3-axis linear stage. The position coordinates provided by the stage were considered as the ground truth and the position

coordinates provided by ROS were evaluated against them. With the improved version of the URDF file, the version used through this thesis, the accuracy and repeatability of the arm was 0.27 mm and 0.95 mm, respectively. Since the accuracy of the arm is smaller than the average US accuracy (≃1mm), it was then demonstrated that the arm will not be a limiting factor in the final results obtain with the system and as such, the arm is suitable to be used as an US probe tracking system in the medical field.

3.1.2 Workflow

The ultrasound scanner used in this project was an EPIQ 7 xMATRIX (Philips) US console. Most of the thesis was done using the X5-1 matrix probe (Philips, 5-1 MHz) and only the ex-vivo and clinical experiments at the end were performed with the L12-3 linear probe (Philips, 12-3 MHz). Scans were acquired from different phantoms and they were streamed in real-time to an US signal receiving PC in a DNL format, which is the streaming format of the EPIQ scanner. From there, and through a socket, the data of the scans was streamed to a ROS PC. The US signal receiving PC in between was needed since at this point of the research it was only possible to connect the EPIQ scanner to a Windows operating system. The US scanner, the US receiving PC and the ROS PC were connected to the same router and data transfer between systems was done via LAN. The position and orientation data of the arm was also streamed to the ROS PC through a microcontroller and via USB. Since the probe was fixed in the probe holder of the arm, the position at which the streamed scans were acquired was known, making possible their visualization in the ROS PC as textured quads. For the needle visualization part (Section 3.3.3), a needle holder was added to the workflow and trough a microcontroller and via USB the insertion depth information was also streamed in the ROS PC. The entire workflow is illustrated in Figure 9.

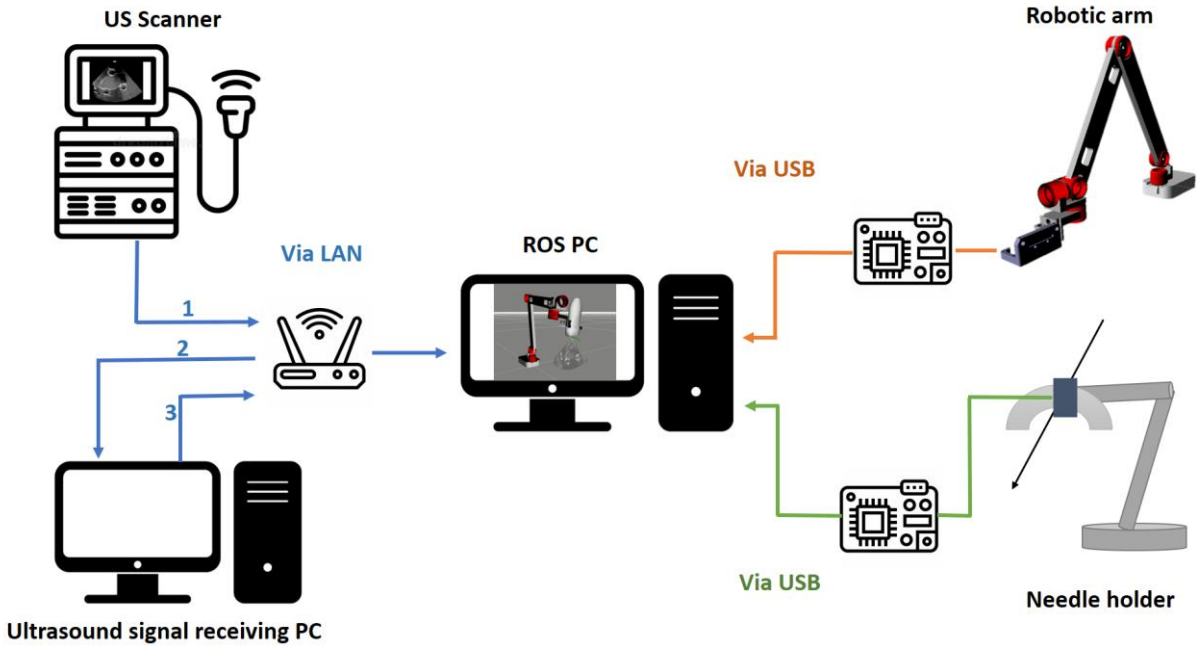

Figure 9. Workflow of the equipment and type of connection between the systems involved in achieving US stitching and biopsy guidance.

3.2 Volume estimation accuracy

Volume assessment is a common procedure in diagnostics and interventional radiology. It was decided to test the reconstruction accuracy of the system by scanning an object of a known volume and compare that volume to the one obtained from the reconstruction. In this experiment, the X5-1 matrix probe and a commercial CIRS phantom (Near Field Ultrasound Phantom, Model 050), with known lesion volumes, were used.

3.2.1 Phantom

The phantom is made of a material called Zerdine, which at room temperature accurately simulates the contrast and attenuation of a human liver as indicated in its datasheet. Inside of the phantom, there are multiple targets and the one of interest for this project is a focal lesion of 21.0 cm^3. This lesion is more echogenic than the surroundings since it is made from Zerdine with a different contrast compared to the material used for the background. An image of the phantom can be seen in Figure 10A and Figure 10B are presents the xplanes acquired while scanning the lesion. Xplane images are real-time images obtained simultaneously from the longitudinal and transversal plane of the scanned morphology, eliminating the need to rotate the transducer to obtain orthogonal views.

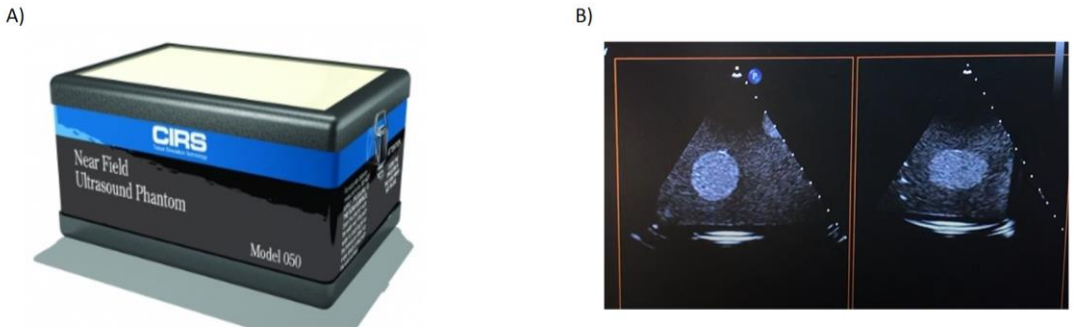

Figure 10. Commercial phantom used to investigate the volume estimation accuracy of the robotic arm probe tracking system. A) An image of the phantom. B) A scan in xplane mode showing an US image of the phantom.

The phantom was scanned combining translational and tilting movements. Tilting movements were mostly incorporated at the endings of the phantom to acquire more data where those are visible since their visibility is lower than the visibility of middle sections of the phantom. The phantom was scanned three times to provide a mean volume value with its standard deviation.

3.2.2 Reconstruction

Streaming the acquired US scans and stitching them using the synchronously streamed position and orientation coordinates of the robotic arm is a computationally expensive procedure. In order to make this procedure less computational expensive, a volume at a predefined position relative to the base of the robotic arm and of a size that includes the phantom was defined and called work area. Only pixels of the US scans acquired in this volume were included in the reconstruction. These pixels were translated into voxels of 1mm x 1mm x 1mm size, making the assumption that this is an approximation that leads to realistic results. At the beginning of the data acquisition, all the voxels in the work area were defined with an intensity value equal to zero and this value was updated when an ultrasound scan with a pixel at this position above a threshold was obtained. This threshold was directly defined to be equal to 0.5 since the contrast difference between the lesion and background of the phantom was clear and the sonographer

could tune the intensity in the scanner. Furthermore, the voxels of the work area had an associated index and thus, when the US scans were accumulated in the volume, only the intensity values were saved and not their coordinates. In this way, the pixels of the scans obtained at the same position were saved only once, decreasing more the computational power required. Another algorithm was developed that checked all the voxels in the work area and provided the coordinates of only the voxels with an intensity higher than 0.5 by relating the indices of the work area to their respective 3D coordinates and saving them into a point cloud. In this way, only memory for the position coordinates of the lesion had to be allocated and not also for the less echogenic parts of the background.

Next, an algorithm to estimate the volume of the reconstructed lesion was tested. This algorithm consisted in a first cleaning stage where only the voxels that form the lesion were saved and the voxels above the 0.5 threshold which corresponded to reflections at the top and bottom of the phantom or to surrounding objects included in the phantom that entered in the FOV of the scans were removed. To achieve that, a rectangular prism of a size that encapsulates the lesion inside was defined. The prism was moved across the work area and the mean intensity value of all the voxels inside of the prism at the different positions was saved. It was assumed that the position at which the mean intensity is the highest corresponds with the position on which the whole lesion was included in the prism since the lesion was the biggest object with high contrast present in the work area. Therefore, the voxels that were outside of the prism at that position were set to zero. Now a closing algorithm was applied to fill in all the holes in the shape and estimate its value by calculating the number of voxel with an intensity higher than 0.5. This number will be equal to the volume of the lesion in mm^3 since as mentioned, the volume of each voxel was equal to 1 mm^3. The chosen structuring element for the morphological operation was a sphere with a diameter of 5 mm since it was expected to have holes of this size with a spherical shape. A closing operation consists of applying the same number of dilations and erosions. There are two different ways of applying a closing algorithm and the selection of one or another depends on the sought end goal. When the goal is to fill holes, all the intended dilations are applied one after the other and to the resulted shape are applied the same number of erosions. However, when the goal is to smooth the object after each dilation an erosion is applied. The first approach was applied in this case since the goal was to fill in the holes of the reconstructed object. The object's volume was calculated 3 times.

3.3 Biopsy needle guidance

In a more realistic case than in the previously used commercial phantom, there are structures such as vessels or other organs close to the lesion from which the physician is planning to take a biopsy. These structures should be taken into account during the biopsy needle path planning to avoid their damage. In this part of the thesis, two phantoms that mimic lesions surrounded by vessels were made, an algorithm that shows all the possible needle paths that do not damage any of the vessels was developed and the needle was visualized in real-time US images.

3.3.1 Phantoms

Ultrasound phantoms can be made with the main intention of mimicking the echogenic appearance of tissues or to also mimic the acoustic properties of those specific tissue types, such as average attenuation, speed of sound, etc [31]. The second ones are either time-consuming or expensive to produce and are mainly used for studying the interaction of sound with tissue or for the assessment of US equipment [31]. Due to the scope of this thesis, it was decided to make phantoms that mimic only how the tissue and lesions would look like in a US scan but it was not intended to mimic also other acoustic properties.

The objective was to develop a prototype to illustrate the suitability of the robotic arm for biopsy guidance. Two phantoms that mimic lesions with surrounding vessels were made using gelatin, copper tubes (which were removed afterwards, leaving holes mimicking vessels) and two different scattering particles. The scattering particles were added to create a material with scattering properties similar to tissues.

The lesions of the first phantom were made by mixing 200 ml of boiling water with 30 g of 175-bloom gelatin from porcine skin (Sigma) and 1.6 g of aluminium oxide (Al_2O_3) particles (Sigma). A beaker of 500 ml was placed on a stirring machine containing water and the gelatin was added in steps to avoid the formation of lumps and facilitate its solubility. 500 rpm were chosen for the stirring, not a very high speed to avoid the formation of bubbles. To facilitate even more the solubility of gelatin in water, the stirring machine was set to 60 °C. Once that all the gelatin dissolved in water, the desired amount of Al_2O_3 was added. Two balloons and a finger of a rubber glove were filled in with the mixture. A syringe was used to measure the introduced volume in the balloons and glove, resulting in three lesions of 30ml, 20 ml and 10 ml. Once the lesions had a room temperature, they were placed in the fridge for 1 hour. Meanwhile, the background tissue, parenchyma tissue, was prepared by mixing in the same way 1.5 L of boiling water, 225 g of gelatin and 1.5 g of Al_2O_3 particles in a beaker of 2.5 L. A summary of the concentrations used in the phantom for the background and the lesions expressed in weight per weight percentage is shown in Table 2. The parenchyma mixture was left to cool down to room temperature and when the lesions were solid, they were taken out of the fridge and the rubber of the balloons and the glove was removed. The phantom was built in one step, not in a multi-layer way, in order to avoid the appearance of bubbles in the interference between different layers. Thus, two copper tubes of 1.2 cm outer diameter were placed at the same height and one next to the other to create a support for the lesions, as it can be seen in Figure 11. A third tube was placed on the top of the lesions to make the access to the lesions more difficult. Oil was spread over the tubes with the use of a paper to make their posterior removal easier. Once that all the parts of the phantom were placed in the desired positions, the container was filled with the parenchyma tissue mixture. The phantom was left in the fridge for one day to solidify and then, the copper tubes were carefully removed. The remaining holes were mimicking the vessels and the phantom was submerged in water to mimic also the blood inside.

Table 2. Concentration of gelatin, Al_2O_3 particles (phantom 1) and Metamucil (phantom 2) for the background and the lesions expressed as weight per weight percentage of the water.

	Background		**Lesions**	
	Weight per weight % gelatin	Weight per weight % scattering particles	Weight per weight % gelatin	Weight per weight % scattering particles
Phantom 1	15	0.1	15	0.8
Phantom 2	15	2.5	15	9.5

Figure 11. Phantom using Al_2O_3 as scattering particles before being filled with the parenchyma tissue mixture.

A second phantom was made following exactly the same procedure but instead of using Al_2O_3 particles, Metamucil was used. Metamucil is a psyllium hydrophilic mucilloid fiber [31] used in many cost-effective tissue-mimicking ultrasound phantoms [31][32][33][34]. The advantage of using Metamucil is that once that the initial mixture is prepared, additional stirring is not needed to maintain a homogenous suspension of the particles and avoid their precipitation [31]. The same quantity of water and gelatin was used as for the previous phantom but in this case, to the lesions mixture 19 g of Metamucil were added and to the parenchyma mixture 37.5 g were added. A description of these concentrations in weight per weight percentage can be found once again in Table 2. It was intended to have a large Metamucil concentration difference between both mixtures but the lesion mixture started becoming thick and that was going to lead to the formation of bubbles while aspiring the mixture with the syringe and introducing it in the balloons and glove. Thus, it was decided to keep a low concentration difference of Metamucil. Also in this phantom, the volume of the three lesions was 10ml, 20 ml and 30ml and once that the tubes were removed, the phantom was submerged in water.

3.3.2 Reconstruction and needle path planning

The phantoms were scanned with the X5-1 probe in xplane mode fixed in the probe holder. A recording that includes both xplanes and the position coordinates of each one of them was acquired using the *rosbag record* function. When the rosbag recording of the phantom was played back using the *rosbag play* function, a node that converts the recorded textured quads into .png images with the use of some OpenCV functions was run. OpenCV is a computer vision library that can be used together with ROS for some purposes. The images were named with their timestamps.

The scans to segment were selected by visual inspection and two approaches were followed to allow comparison. In the first approach, the lesions were segmented once every ten frames to have a lot of data for their reconstruction. Although it was a repetitive and time-consuming method since the segmentation of each scan took 30 to 40 seconds, it was done to obtain an empirical estimation of the phantom considered to be close to the ground truth. In the other approach, it was decided that each lesion was going to be segmented from one scan that visualizes the start of the lesion, one that visualizes the middle of the lesion and one that visualizes the end of the lesion. Additionally, each lesion was also segmented from one scan from the other xplane, and then perpendicular to the other three segmented scans, that included the whole lesion. The lesions were segmented in MATLAB with the use of the *imfreehand()* function and the vessels were segmented with the *imellipse()* function. It was decided to use *imellipse()* for segmenting the vessels since their cross section looked always circular in the US images and with this function better segmenting results were achieved than manually segmenting them. Once that the cross sections were segmented, a mask englobing this segmentation was created. Colours represented the object labels and in order to give different colours to the masks of the lesions and the vessels, the individual RGB channels of the images needed to be extracted and set to the desired value. Once that was done, the RGB individual channels were recombined in a single true colour RGB image. The chosen colours for the masks had always a 255 value for the green channel. An example of a segmented US scan of the phantom made with Metamucil is given in Figure 12. It is possible to observe that the contrast difference between the background and the lesions in this phantom was small. This

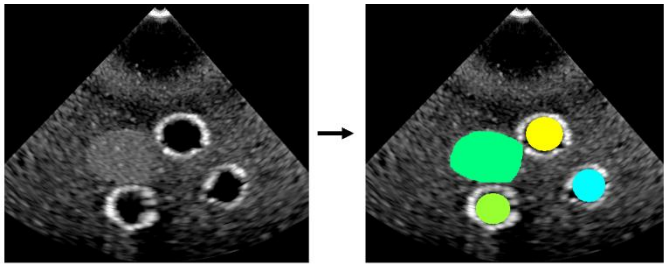

Figure 12. US scan acquired from the phantom made with gelatin and Metamucil and its segmentation.

made the segmentation complicated in some frames but it illustrated a case close to the observed one in a clinical scenario. The segmented images were saved and named with their timestamps followed by a _X1 or _X2 ending indicating to which xplane they belonged.

Once again, a work area of a size and at a position with reference to the base of the robotic arm that includes the scanned phantom was generated. The rosbag was played again and a node was checking if there was a segmented image with a name that corresponds to the current timestamp of the recording. If so, it also checked the name of the image to see to which xplane corresponded since a coordinate system for both xplanes was defined. In total, there were three lesions and three vessels, then six different elements segmented with 6 different colour labels. Since for all the segmented parts in the images the green channel was equal to 255, it was possible to implement an if statement that only includes in the next steps pixels whose green channel value was equal to 255. This was implemented to speed up the algorithm and avoid unnecessary processing. At the beginning, the intensity values of all the voxels in the work area were equal to zero. The if statement checked which pixels in the US scans corresponded to which elements and updated their corresponding intensity voxels values in the work area with a specific and unique value for each element ranging from 0.2 to 1.0. The assigned intensities are specified in Table 3. In essence, this was a relabelling of the segmented elements from the 2D US scans to their position in the 3D space. For one of the lesions it was studied the reconstruction difference between defining the voxels with a 1x1x1 mm size and defining them with a size almost equal to the scaling factor of the scans (0.2x0.2x0.2 mm). This was highly computational expensive and a work area only around the studied lesion had to be defined.

Table 3. Assigned intensities in the work area to the elements present in the phantoms.

	Vessel 1	**Vessel 2**	**Vessel 3**	**Lesion 1**	**Lesion 2**	**Lesion 3**
Intensity	0.2	0.4	0.6	0.5	0.8	1.0

When the segmented US scans were displayed in the ROS 3D space, another node that goes along the whole work area and checks the intensities of the voxels on it was run. An if statement in this node was the responsible of saving the position coordinates of the different phantom elements in different .txt files. In total, 6 .txt files were generated, 3 files for the three lesions and 3 files for the three vessels. Each .txt file contained the points data set that form the associated element.

These .txt files were imported in MATLAB where the *alphaShape* function was used. For a given set of points, an alpha-shape is created from a subcomplex of the Delaunay triangulation [35]. The alpha parameter is the one that regulates the level of refinement. A large alpha results in a coarse fit (a convex hull) while a smaller alpha results in a finer fit [35]. Determining the value of this parameter is the key point of the algorithm since it can provide very different outputs as it can be observed in Figure 13. In this study, the best results were observed with an alpha value of 3 for the lesions and the vessels. In Figure 14 it is possible to see the 4 scans manually segmented from the phantom made with Al_2O_3 particles, how they look like in the 3D space when the position data from the arm is used and the result obtained with the alpha-shape algorithm. The same workflow was followed when 1 every 10 scans were used for the reconstruction. The only difference is the number of scans used for the generation of the alpha-shape. It can be appreciated in the US scans in Figure 14 that the lesions in this phantom presented a contrast gradient due to possible precipitation of the Al_2O_3 particles that made complicated the definition of the lesion's edges. The same reconstruction workflow was also used for the phantom made with Metamucil.

Once that the alpha shapes were obtained, it was possible to save them as .stl files and import them in ROS at their original coordinate system. Furthermore, it was possible to calculate the centroids of the

lesions by using the function *centroid* in MATLAB and in the case of the vessels, it was possible to calculate all the 3D points inside them by using the *inShape* function, which checks if a given value belongs to inside of the alpha-shape or not. The 3D points that form the vessels were found by checking the 3D points of the work area with the *inShape* function. Next, they were saved in .txt files and imported back in ROS. The repeatability of the calculated centroids was studied by acquiring multiple recordings of the same phantom without moving the base of the arm or the phantom so the spatial relation between them is kept. Furthermore, the estimated centroid with the 4 frames approach was compared to the centroid obtain through the empirical approach to test the performance of the 4 frames method.

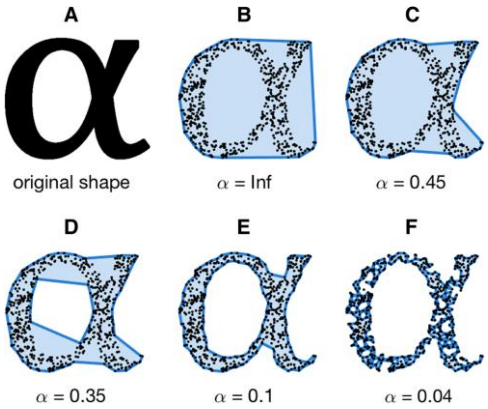

Figure 13. Illustration of the possible results to obtain while using the alpha-shapes algorithm with different values for the alpha parameter [35].

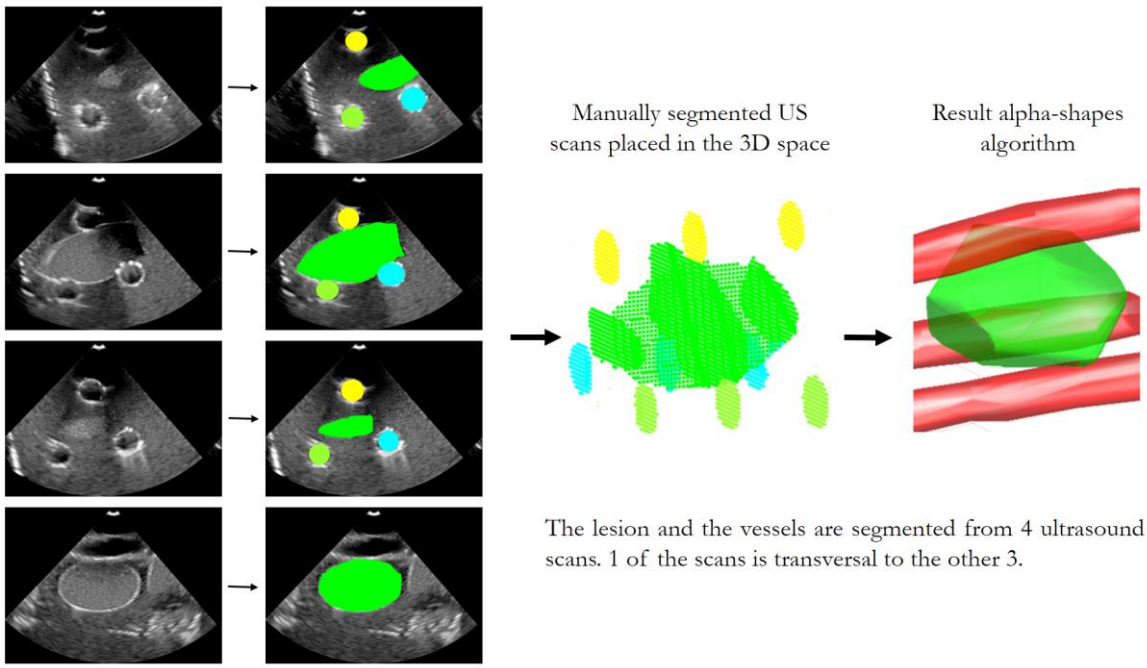

Figure 14. Steps involved in the reconstruction. Firstly, the lesion and the vessels are manually segmented from both xplanes. Secondly, the segmented areas are placed in 3D space thanks to the position coordinates provided by the robotic arm. Finally, the scans are interpolated with the use of the alpha-shapes algorithm and the phantom is reconstructed.

A transform was defined at the start of the US probe and it was going to be supposed that this point corresponds with the top of the phantom and that in the future, it will correspond with the skin surface of the patient. One of these points was going to be the access point of the biopsy needle and therefore,

the position and orientation coordinates of this transform were saved. In Figure 15 it is possible to see where exactly this transform was defined.

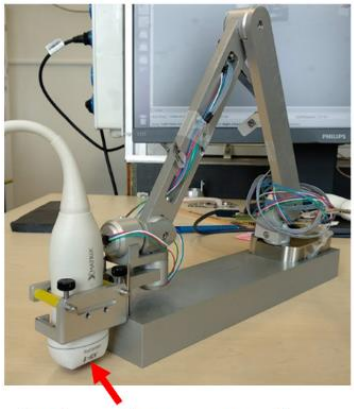

Figure 15. Illustration of where the surface phantom transform was defined.

The goal was to take a biopsy sample from the centre of the lesion without damaging any surrounding vessel. Then, all the lines that connected the centroid of each lesion with one of the points at the top of the phantom were evaluated and only the ones that do not pass close to any vessel were considered as possible needle paths. Considering a line that passes through the points A and B and having a point C as illustrated in Figure 16A, the shortest distance between them is always the perpendicular distance, CP. If now a parallelogram ABCD is formed as shown in Figure 16B, CP is going to be the height of that parallelogram. Hence the area of the parallelogram is equal to the cross product of AB and BC, and it is also equal to the base multiplied by the height, AB*CP, it is then possible to calculate the shortest distance, CP, as indicated in Equation 1 Taking this into account and checking the minimum distance between the lines that connected the centroid with the points at the top of the phantom and the points that form the point cloud of the vessels, it was possible to implement an algorithm that only shows the paths that do not pass next to a vessel below a threshold. In this case, this minimum distance threshold was selected to be 2 mm. From these possible needle paths, it was also possible to select the one with the shortest length by calculating the Euclidian distance between the two ending points as indicated in Equation 2. The resulting path would be the needle path that punctures the fewest amount of tissue.

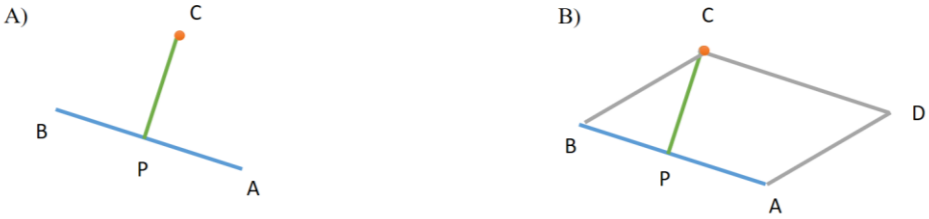

Figure 16. Shortest distance between a line and a point. A) Having a line that passes through the points A and B and a point C, the shortest distance is the perpendicular distance, CP. B) By constructing the parallelogram ABCD and calculating its area, it is possible to calculate CP.

$$Area = |AB| * |CP| = |\,AB\ x\ BC| \ \rightarrow CP = \frac{|AB\ x\ BC\,|}{|AB|} \qquad (1)$$

$$d = \sqrt{(x_1 - x_2)^2 + (y_1 - y_2)^2 + (z_1 - z_2)^2} \qquad (2)$$

3.3.3 Needle visualization

A setup available at Philips Research and initially designed for local anaesthesia needle guidance was used as a proof of concept for the demonstration of how the biopsy needle could be visualized in the

system. This setup can be considered as a needle holder. The probe holder of the robotic arm was attached to it in such a way that the needle will always be in plane with the US beam and therefore, the needle will be visualized in the US image. The needle holder includes an angular stage that allows changing the angle between the probe and the needle and a linear stage that controls the depth at which the needle is placed. It was possible to read the values of the linear stage and stream them to the ROS PC. A container with water was placed below the robotic arm and the water level was at the same height as the US probe, making the visualization of the needle possible. An absorption rubber material was placed at the bottom of the container to avoid reflections that otherwise could create unwanted artifacts in the images. The whole setup can be seen in Figure 17A and a closer look of the needle holder in Figure 17B.

To get the correspondence between needle insertion measurement coming from the encoders of the linear stage and real displacement, the needle was displaced to 10 different position and the measurement values and real displacement measured with a caliper were noted down. The mean obtained value from the 10 positions was considered as the correspondence between measurement value coming from the encoders and real displacement. The distance between the point of rotation of the needle with the angular stage and the transform defined at the start of the probe was measured with the help of a caliper. A new transform was defined at the rotation point since this point will not change in space when the needle is rotated with respect to the probe. It was now measured with a caliper the distance between the rotation point and the tip of the needle when the needle is placed at a preselected depth. This measurement indicates the position of the tip of the needle and will be updated with the real-time data coming from the linear stage.

ROS allows the visualization in RViz of shapes such as lines, squares, spheres, etc. This shapes are called markers. A line marker was defined from the transform to the measured position of the tip and the length of this marker was updated with the values streamed by the linear stage in such a way that one of the endings of the marker was always representing the real-time position of the needle's tip. An observation is that the values provided by the linear stage were relative and thus, they depend on the position of the needle when the node is initialized. It was then needed to start the node when the needle was at the same preselected position in terms of depth to correctly update the needle's depth indicated by the marker. The position of the needle's tip was verified by overlapping with the marker streamed real-time US scans as textured quads. The needle was moved to confirm a good overlap during the whole insertion path. The evaluation was performed over four different insertion angles, 45°, 50°, 55° and 60°.

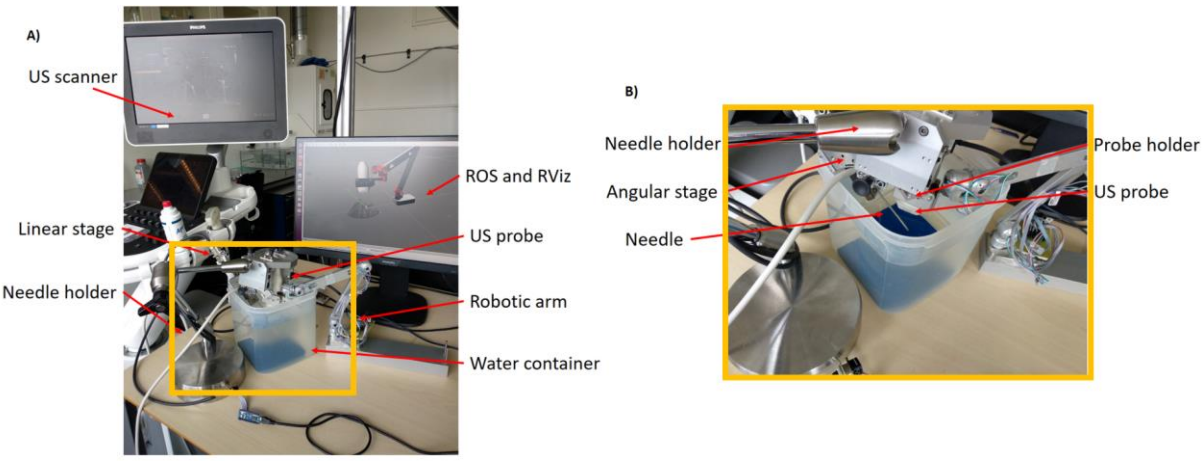

Figure 17. A) Whole setup used for tracking in real-time the tip of the needle. B) A closer look to the setup, properly visualizing the needle.

3.4 Vessel reconstruction in an ex-vivo and clinical evaluation

3.4.1 Setup and protocol

The usability of the robotic arm as an US tracking system for imaging large parts of vessels was also investigated. This was done through an ex-vivo study using a pork leg and a pilot study performed on two subjects. In this case, an additional probe holder previously designed for the linear probe L12-3 (Philips) was mounted on the probe holder designed for the X5-1 probe. The translation between both probe holders was measured with a caliper and resulted in a translation of (0, 4.84 , 6.55) cm.

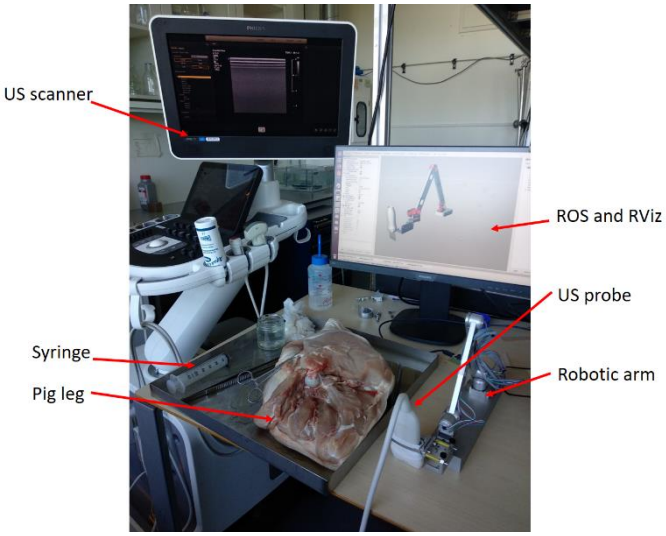

Figure 18. Setup used for the ex-vivo study with a pork leg.

Different areas of the pork leg where scanned with the linear probe attached to the robotic arm in order to find some vessel which to track. However, it was not possible to visualize the vessels of the pork leg since they were collapsed as a result of no blood flow. Therefore, it was decided to find some of the major vessels and manually inject water inside with a syringe while scanning the vessel. That made possible the visualization of a small part of the localized vessel. In Figure 18 it is possible to see the whole setup.

Additionally, the forearm of two subjects were scanned. In this case, it was easy to track multiple vessels over a large space. The scanning protocol consisted of finding major vessels and tracking them along the forearm by moving the probe to positions that provide a cross-sectional view of the vessels.

3.4.2 Reconstruction

The reconstruction consisted of the same stages like the ones described in Section 3.3.2. A recording of the desired volume was acquired and from which all the US scans were exported. The vessels were manually segmented in MATLAB and the segmented areas were placed in the 3D space by using the position and rotation coordinates provided by the arm and adjusting the size and position of the work area. The 3D coordinates of the segmented vessels were imported to MATLAB, once again, where their alpha-shape was reconstructed. Figure 19A shows an US scan obtained from the pork leg and the segmented vessel. The bifurcation occurring in this vessel is not well visible directly on the 2D US images. However, the morphology of the reconstructed vessel gave insights about the existence of the bifurcation. By reviewing again the scans, the second vessels of the bifurcation was also identified and the segmentation of both vessels is shown in Figure 19B. Additionally, Figure 20 shows an US scan acquired from subject 1 and the segmentation of the vessel present on it.

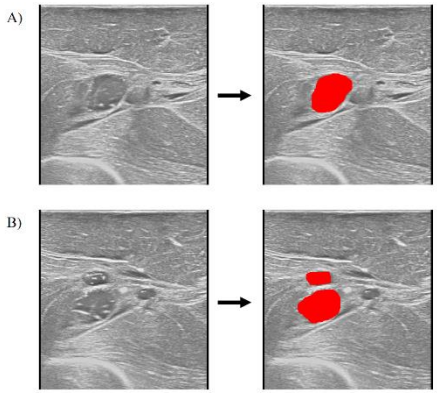

Figure 19. US scans obtained from a pork leg. A) An US scan where it is possible to see a major vessel and its segmentation. B) An US showing the bifurcation of the vessel in A) and its segmentation.

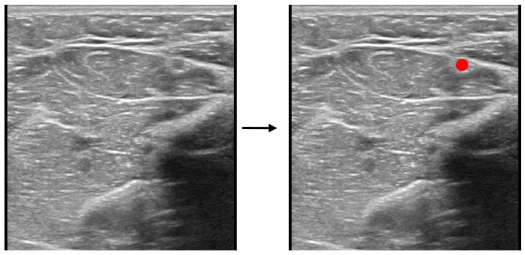

Figure 20. US scan obtained from subject 1 and the segmentation of the vessel present on it.

3.5 Development of an automatic or semi-automatic segmentation algorithm

Attempts to develop an automatic or semi-automatic segmentation algorithm of shapes were performed. It was intended to develop a not highly computational expensive algorithm that can provide a result in a short time or, ideally, in real-time. The investigation of possible ways to achieve this objective was done in MATLAB by using already available functions.

3.5.1 Phantoms

The phantom used for the development of an automatic or semi-automatic algorithm consisted of a previously available 3D object with the shape of a dinosaur, made of PVA and aluminium oxide particles, inserted in gelatin. The mixture of gelatin was prepared by mixing with a stirring machine 1.3L of boiling water with 200g of 175-bloom gelatin (Sigma) – ~15 weight per weight percentage mix. The phantom was made in two stages. Firstly, a layer of the mixture was poured in the container and it was introduced in the fridge to cool down. During this period, the rest of the mixture was kept on the stirring machine at a temperature of 40°C in order to avoid its solidification. Later, when the layer was solid, the container was taken out of the fridge, the dinosaur was placed on the layer and the remainder of the mixture was added to the container. The container was introduced again in the fridge to cool down and solidify. The result can be seen in Figure 21A. Once solid, the phantom was taken out of the container and scanned with the X5-1 probe (Philips) fixed in the robotic arm. Since the phantom was made in a two layer approach, bubbles formed in the interface between both layers and generated artifacts in the US images as it can be seen in Figure 21B.

Figure 21. Phantom used for the development of an automatic or semi-automatic segmentation algorithm. It consisted of a dinosaur shape made of PVA with alumium oxide particles as inclusion in a gelatin mixture. A) Photo of the phantom. B) US image of the phantom.

Additionally, some attempts to develop an algorithm were done with the phantoms described in Section 3.3.1.

3.5.2 Developed algorithms

US images usually contain speckle noise which influence the image appearance and can cause a negative impact in the post-processing of the images. Suppressing this speckle noise is an important preprocessing step before image segmentation. There are various filtering techniques but only the median filter was considered for this project since it is not that computational expensive as the Weiner filter could be, for example [36][37] and it preserves the edges[36]. It was decided to use a neighborhood of 3x3 size since the biggest the neighborhood the more computational expensive is this pre-processing step.

The first attempts to segment the regions of interest (ROIs) in an automatic way consisted in applying different thresholding techniques to divide the pixels in foreground and background based on their intensity values. Firstly, global thresholding was applied on which a threshold value is manually assigned and pixels with higher intensity are considered foreground and pixels with a lower intensity are considered background [36]. Next and to overcome the need of manually selecting a threshold value, it was also studied the possibility of using the Otsu's thresholding method, through which a threshold value is automatically selected [36]. The results of these thresholding techniques were evaluated with and without firstly applying the aforementioned preprocessing step. Additionally, it was also studied the suitability of applying a closing morphological operation to the thresholded images, followed by an opening. The objective of the closing was to fill in the holes in the ROI and the objective of the opening was to remove artifacts around the ROI created by the bubbles. Structuring elements of different shapes and sizes were evaluated but the main focus remained in disc-shaped structuring elements.

It was also explored the possibility of segmenting the ROIs by using an edge detection technique as another automatic segmentation algorithm. To do that, the images were firstly preprocessed by applying a median filter. Next, a masked image was obtained through thresholding (both, global and Otsu were explored) and a closing algorithm was applied to fill in the holes. Now, a Canny edge detection algorithm was applied showing all the boundaries where there was a rapid intensity change. A dilation was applied to close the contours and all the regions were found. Finally, it was supposed that the segmented ROI was the second biggest region since the first biggest region should be the background and assuming that there was not going to be a region bigger than the ROI.

On the other hand, active contours were investigated as a semi-automatic way to segment the ROIs. This technique needs to be initialized by a seed from which the region will keep growing by analyzing the intensity value of the neighboring pixel [36]. In this approach, the images were preprocessed, once again, by applying a median filter. A rectangle that includes the ROI was manually drawn and the Chan-Vese active contour algorithm was applied. It was intended to use this algorithm in a semi-automatic way by following the approach proposed by [24] where they used an electromagnetic tracking system to segment the thyroid glands from images obtain from subjects. In their method, the physician just had to initialize the mask for the first image and the mask of the next images was automatically computed by projecting in the next US plane the centre of mass of the preceding segmented image.

Some of the results of those algorithms can be seen in the Appendix.

4. Results

This chapter presents the results of the experiments as described in the previous chapter. The decision-making process behind choosing this initial clinical application is described in Section 4.1. The process led to the decision that liver imaging for biopsy guidance was going to be the first application. The next step was to demonstrate that with the robotic arm tracking system is possible to accurately reconstruct objects of different shape and size, indicate the possible biopsy needle paths and visualize the biopsy needle in real-time. The results of these experiments are shown in section 4.2 and 4.3. Finally, the performance of the system was tested in an ex-vivo and clinical setup, Section 4.4.

4.1 Selection of initial clinical application for the system

As a first step to solve the first objective of this thesis, finding and selecting a clinical application for the system, the considered applications were categorized for two main purposes, only diagnostics or combination of diagnostic and intervention. The result of this classification is shown in Figure 22.

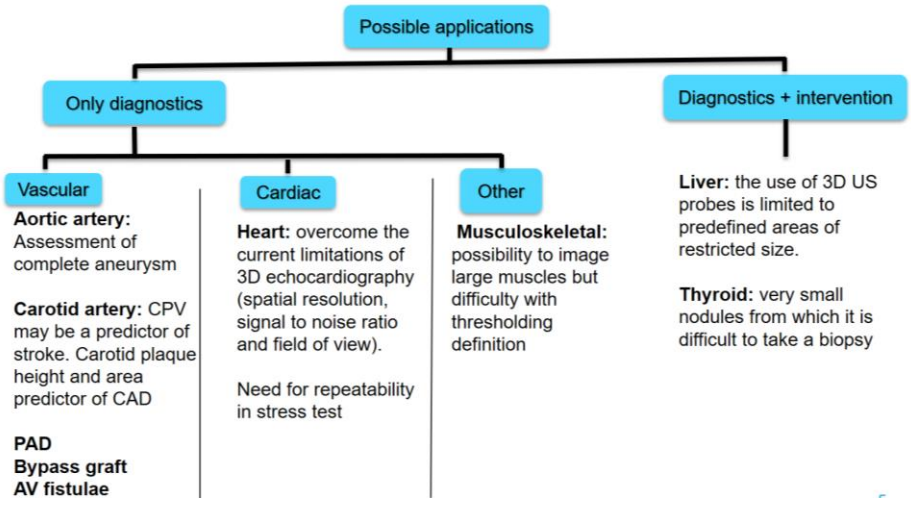

Figure 22. Classification into two main purposes, only diagnostics or diagnostic plus intervention, of the considered applications for the system.

In the group of only diagnostic purposes are included vascular, cardiac and musculoskeletal imaging. The purpose of using the robotic arm for US stitching for these applications would be to provide extended FOV images where all the anatomy and/or pathology can be visualized, decrease operator-dependency and increase the quality of surveillance examinations. Furthermore, merging US scans from multiple perspectives can increase the quality of the images since artifacts present from one perspective may not be present from another perspective. The enhancement of these properties will provide an improved and more accurate diagnosis, a better treatment plan and the avoidance of unnecessary treatments.

As indicated in Chapter 2, the assessment of complete aneurysm with a single 3D scan is not possible in 40-45% of the cases [5]. Therefore, in those cases it is not possible to perform a wall stress analysis. Several studies investigated the fusion of multiple scans using image registration algorithms [5] [7] [9]. The reconstructions obtained using those algorithms when compared to the reconstructions obtained from a different imaging modality showed a good similarity between both. Furthermore, after having a discussion with one of the authors of those research [38]**,** it was possible to understand that the applied image-based registration algorithms perform well when there is enough curvature to track in the volume of interest. That is the case with aneurysms and then it is not that difficult for the algorithm to interpret where to place the next scan in accordance with the morphology observed in the previous scan. Therefore, this application was decided to be discarded since good results are already obtained with this technique and it was perceived that with the robotic arm system it is not possible to provide a much higher improvement.

It was considered that the robotic arm could provide significant improvements for peripheral artery disease, autologous bypass grafts and AV fistulas due to the large volume that needs to be scanned. However, testing the performance of the arm for those applications with a phantom based setting was thought to be difficult. These applications can be better tested in a clinical study involving patients. However, due to the limited time of this master thesis compared to the approval time from an Ethical Committee to perform such study, those applications were also discarded for this research. However, they are applications that should be taken into account in the future, once that the good performance of the system has been proven and that there is more time to organize and set up a clinical study.

Carotid artery imaging was an application considered as feasible to be the first application of the system until one of the last stages of the selections process. However, once again, it was considered that there was not enough research scope in a phantom based setting and it was better to explore that application in a later step with a clinical study comparing the reconstructed CPV with the volume of the endarterectomy specimen, similar to research done by [10].

In the case of musculoskeletal imaging, the robotic arm could provide huge value in the scanning of long muscles where an extended FOV is highly needed. Furthermore, developing such a system based in US imaging could open an interesting US market into the sport's domain. However, identifying the different musculoskeletal structures in an US scan is expected to be complex as also indicated by [29] and thus, this application should not be the initial application with which to test the performance of the robotic arm.

The selected application from the only diagnostic group was cardiac imaging and it was discarded only after the first results obtained for volume estimation accuracy using the robotic arm tracking system. The results of that study are presented in the next section, Section 4.2. The acquisition and processing of the US scans was slow, not instantaneous, and that could be a problem for imaging a moving organ as the heart since vital information could be lost during acquisition. This insight led to the decision of

discarding also cardiac imaging as the initial application for the system. However, cardiac imaging is another application that should be considered in the future.

Liver and thyroid imaging were categorized in the group where diagnostics can be combined with intervention. The clinical idea for those applications consists of combining a biopsy needle holder with the probe holder. The position of the needle in this holder will be known, fixed and in such a way that the needle is always in plane with the US beam and it is then always visualized in the US scan. Therefore the procedure will involve a first extend FOV US scanning of the anatomy of interest. If the physician sees in that scan something suspicious to be a tumor, he will ask the patient if he agrees in undergoing a biopsy in that exact moment. If the patient agrees and supposing that he does not move, it would be possible to guide the needle to the lesion by estimating the optimal path to the lesion without damaging surrounding structures and taking a good sample. This approach is in tone with the one-stop-shop tendency as indicated by an interviewed physician during this thesis work [28]. In one-stop-shop, the diagnostics and the biopsy procedure are performed one exactly after the other. The procedure in liver and thyroid imaging allowing biopsy guidance is basically equal with the difference in organ and lesion sizes.

It was then decided that the initial clinical application of the robotic arm was going to be for liver imaging and biopsy guidance since a huge potential was observed with the use of the robotic arm as a tracking system and in combination with a needle holder, and since it is better to firstly start with an organ that presents lesions of a bigger size. Once its good performance for the liver is demonstrated, it can easily be adapted for thyroid imaging where a very high degree of accuracy during biopsy guidance will be required due to the small size of the thyroid lesions. Furthermore, the prevalence of liver cancer is high and it is expected to achieve better results than the ones obtained by [23] since robotic arm tracking systems are usually more accurate than electromagnetic tracking systems. Also, the arm used in this project provides more freedom to the physician than the automated handheld assembly developed by [22] allowing him to acquire images from exactly the areas where he suspects that a tumor is present.

4.2 Volume estimation accuracy

This section presents the results of the first approach for volume reconstruction and volume estimation. The result of applying a global thresholding algorithm in such a way that only the pixels with an intensity value higher than 0.5 are represented in the 3D space is shown in Figure 23 as grey coloured voxels. Furthermore, with pink coloured voxels are also illustrated the voxels corresponding to the egg-shaped object of interest obtained after cleaning the data and applying four times a morphological closing algorithm as described in Section 3.2.2. The reconstructed volume was equal to 20.3±0.5 ml while the indicated volume of the object in the datasheet of the phantom was 21.0 ml. Thus, the reconstructed volume was slightly smaller than the actual volume but comparable, showing the good performance of the system for reconstructing the shape and volume of objects. However, the acquisition and processing method of this algorithm was time-consuming and it indicated that the first application with which the system would be tested should involve preferably the imaging of a static organ and not the imaging of a moving organ as the heart.

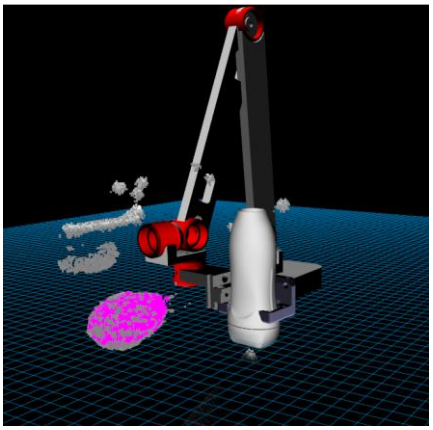

Figure 23. Reconstructed phantom volume. In gray are indicated the voxels with an intensity higher than 0.5 and in pink the obtained voxels after applying the cleaning data box and four morphological closings, resulting in a reconstructed volume of 20.3±0.5 ml.

4.3 Biopsy needle guidance

4.3.1 Phantom reconstruction

Firstly, the reconstructed egg-shaped object in Section 4.2 was reconstructed by manually segmenting the object from multiple frames and interpolating them with the alpha-shapes algorithm. Since the phantom was scanned by slowly moving the probe, a lot of US frame data was available for almost the same parts of the phantom. It was then decided to segment the object once every 20 frames acquired in the recording. This resulted in the segmentation of 37 frames including cross sections of the phantom, corresponding to the X2 xplane, and 2 frames including transverse sections, corresponding to the X1 xplane. The frames were interpolated by applying the alpha-shapes algorithm with an alpha value equal to 3 and the result is presented in Figure 24. The origin of all the results presented in this chapter was defined at the base of the robotic arm and thus, in Figure 24 it is also possible to see the position of the egg shape with respect to the base of the robotic arm. In this case, the reconstructed volume was equal to 22.1 ml.

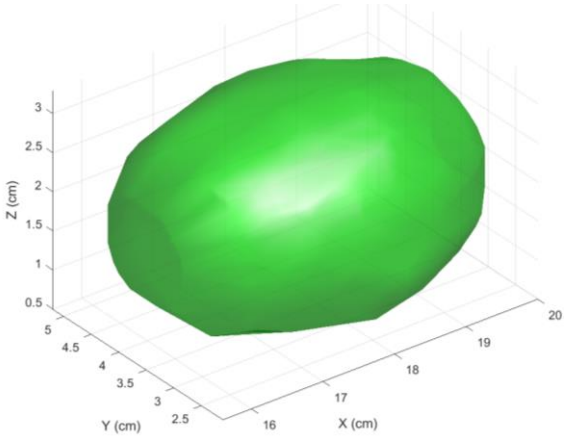

Figure 24. Reconstructed egg-shaped object through manual segmentation of several US scans and interpolation with the alpha-shapes algorithm.

Next, the phantom made with gelatin and Al_2O_3 particles including lesions and surrounding vessels was segmented. The three included lesions have been enumerated as indicated in Figure 25 and a photo of the phantom is shown in Figure 25A. In total, there were 3 recordings available of this phantom. In the first recording, all the lesions were well visible and its reconstruction when segmenting 1 every 10 frames is shown in Figure 25B and the reconstruction when segmenting 4 frames per lesion in shown in Figure 25C. In both cases, an alpha value equal to 3 was used for the vessels and lesions. A blue dot indicates the estimated centroid in those reconstructed alpha-shapes.

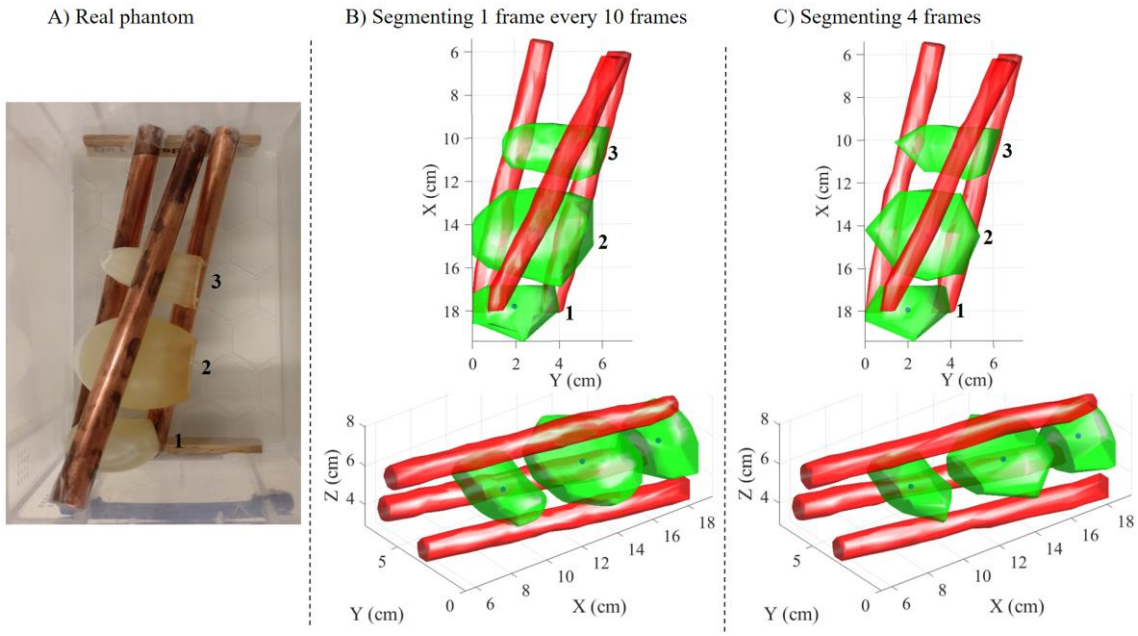

Figure 25. Reconstruction of the phantom made with gelatin and Al_2O_3 particles. A) A photo of the phantom. B) A reconstruction of the phantom by segmenting the lesions and vessels from 1 frame every 10 frames. C) A reconstruction of the phantom by segmenting 4 frames per lesion – 3 X2 xplanes containing the beginning, middle and end of the lesion and one X1 xplane perpendicular to the other 3 scans. The blue dot indicates the centroid of each lesion.

Lesion 1 was very close to the ending of the phantom, which resulted in the appearance of artifacts in the US scans. An acceptable reconstruction of this lesion was achieved only from the first recording. Furthermore, the base of the robotic arm moved between the first and second recording, resulting in a different origin and thus, the results obtained for the coordinates of the lesions centroid were only comparable between the second and third recording. The results presented in Table 4 correspond to the mean volume and mean centroid coordinates of the two well visible lesions, lesion 2 and lesion 3, in the second and third recording. The repeatability of the method based on the standard deviation of the lesions centroid estimated from different recordings is not presented for this phantom since only two recordings were analized. In total, 31 X2 xplanes and 2 X1 xplanes for lesion 2 in the second recording and 39 X2 xplanes and 2 X1 planes in the third recording were segmented. For lesion 3, 19 X2 xplanes and 2 X1 xplanes were segmented in the second recording and 20 X2 xplanes and 2 X1 xplanes in the third recording.

Table 4. Mean reconstructed volume and mean position coordinates of the lesions centroid for lesions 2 and 3 in the phantom with Al_2O_3 particles when for the reconstruction are used 1 frame every 10 frames or 4 frames.

	Lesion 2	**Lesion 3**
Real volume (ml)	30	10
Mean reconstructed volume segmenting 1 frame every 10 frames (ml)	36.2	13.3
Mean centroid segmenting 1 frame every 10 frames (cm)	(16.66 , 3.68, 5.20)	(12.81, 4.55, 4.54)
Mean reconstructed volume segmenting 4 frames (ml)	28.2	12.1
Mean centroid segmenting 4 frames (cm)	(16.75, 3.91, 5.17)	(12.93, 4.99, 4.59)

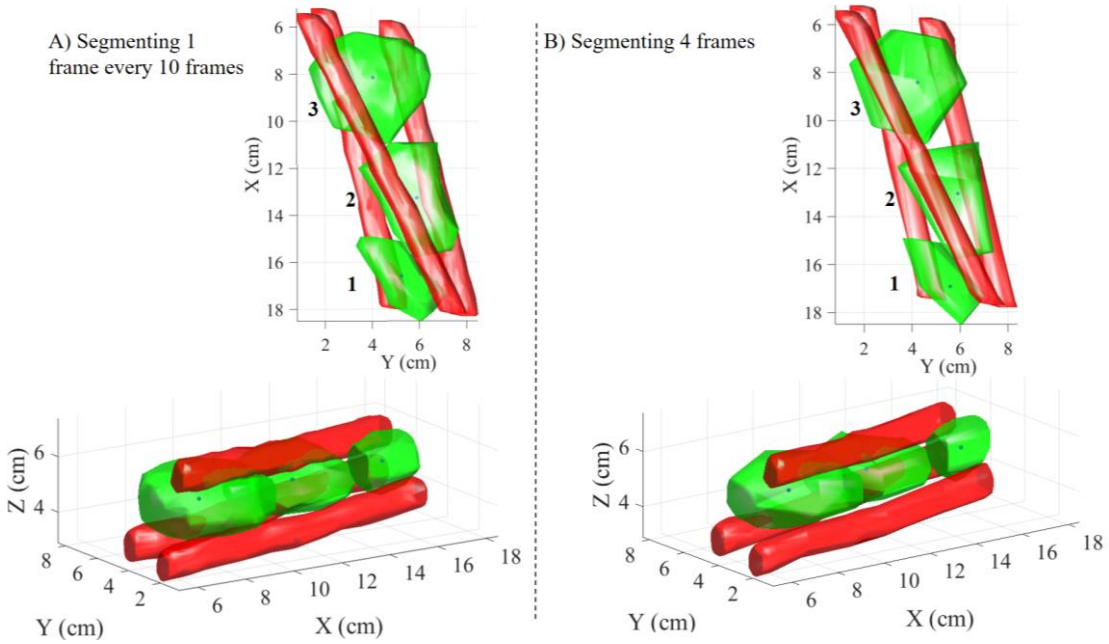

Figure 26. Reconstruction of the phantom made with gelatin and Metamucil. A) A reconstruction of the phantom by segmenting the lesions and the vessels from 1 frame every 10 frames. B) A reconstruction of the phantom by segmenting 4 frames per lesion – 3 X2 xplanes containing the beginning, middle and end of the lesion and one X1 xplane perpendicular to the other 3 scans. A blue doth indicates the centroid of each lesion.

In the case of the phantom made with gelatin and Metamucil, 4 recordings were acquired and the three lesions were well visible in all of them and enumerated as indicated in Figure 26. It was then possible to estimate the mean volume and the mean position coordinates of the centroids of the three lesions and provide their standard deviations as a repeatability indicator. When segmenting 1 scan every 10 scans, 11 X2 xplanes and 1 X1 xplane were segmented on average for lesion 1 from the four recordings. For lesion 2, 17 X2 xplanes and 1 X1 xplanes were segmented on average and lesion 3 was segmented on average from 24 X2 xplanes and 1 X1 xplane. The results in Figure 26A correspond to the reconstruction that was obtained by segmenting 1 scan every 10 scans while Figure 26B shows the results when only 4 frames per lesion were segmented. Both Figures were obtained from the second recording and by using an alpha value equal to 3 for both, lesions and vessels.

Table 5 summarizes the results of the 4 recordings. The 3D coordinates of the lesions' centroid could be estimated with a repeatability of less than 1 mm across repeated phantom scans for 72% of centroid coordinates in 3D space. When comparing the estimated lesions' centroid coordinates in both phantoms obtained by segmenting 1 every 10 frames and segmenting 4 frames per lesion, a difference smaller than 1 mm was observed for 60% of the centroid coordinates and a maximum difference of 4 mm was observed for one of the lesions' centroid coordinates. The resulting five reconstructed lesions in both phantoms showed volume overestimation in almost all evaluated cases with an average percentage error of 14.6%. The volume of lesion 3 in the phantom made with Metamucil calculated by decreasing the voxel size of the work area and making it almost equal to the scaling factor of the US scans (0.2mm x 0.2mm x 0.2mm) was equal to 33.0 ml.

Table 5. Mean reconstructed volume and mean centroid of the lesions with their standard deviation for the phantom with Metamucil when for the reconstruction are used 1 frame every 10 frames or 4 frames.

	Lesion 1	**Lesion 2**	**Lesion 3**
Real volume (ml)	10	20	30
Mean reconstructed volume segmenting 1 frame every 10 frames (ml)	10.6±0.8	19.6±0.9	33.4±0.8
Mean centroid segmenting 1 frame every 10 frames (cm)	(16.53±0.05, 5.18±0.07, 4.93±0.03)	(13.21±0.06, 5.87±0.02, 4.60±0.03)	(8.33±0.18, 4.03±0.02, 4.98±0.06)
Mean reconstructed volume segmenting 4 frames (ml)	8.4 ± 1.0	15.4 ± 2.5	28.2 ± 1.2
Mean centroid segmenting 4 frames (cm)	(16.57±0.35, 5,42±0.18, 4.84±0.10)	(12.99±0.06, 5.79±0.13, 4.54±0.03)	(8.38±0.04, 4.32±0.09, 4.97±0.04)

4.3.2 Needle path planning

Once that the phantom is reconstructed, it is possible to evaluate all the paths that connect the centroid of one of the lesions with one of the points on the surface of the phantom and do not lead to a vessel damage, representing possible needle paths. Figure 27A shows in cyan all the possible needle paths for the second lesion in the phantom made with gelatin and Al_2O_3 particles and reconstructed from 4 frames that comply to the constraints and Figure 27B shows the shortest of all these possible needle paths. In both figures, the points on the top of the phantom are illustrated with green dots.

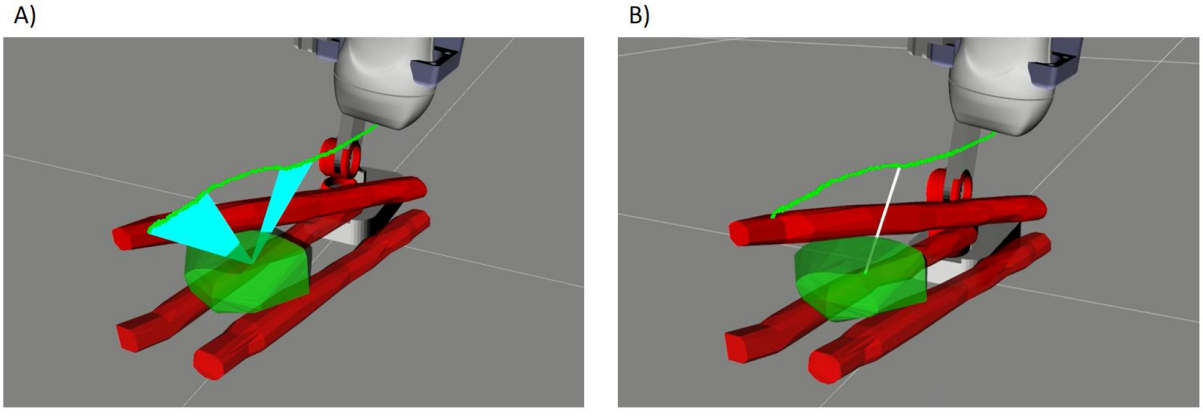

Figure 27. Possible needle paths. A) With cyan lines are shown the needle paths that conect one of the points on the top of the phantom with the centroid of the lesion and do not pass next to a vessel closer than 2 mm. B) With a white line is ilustrated the shortest path from the ones shown in A). The green dots show points on the surface of the phantom.

4.3.3 Needle visualization

Once that the phantom is reconstructed and the best needle path is calculated, it is possible to guide the needle to the centroid of the lesion by overlapping real-time US imaging with a line marker whose length is updated in real-time, showing always where the tip of the needle is. The obtained correspondence between needle insertion measurement coming from the encoders of the linear stage and real displacement was 0.39 ± 0.1 µm/measurement. It was possible to see a correspondence between the position of the tip indicated by the line marker, the position seen in the US scan and how this correspondence was maintained along all the insertion path. Figure 28 illustrates the overlap for four different insertion angles, 45°, 50°, 55° and 60°. Visually the correspondence appears correct but a quantification of the accuracy is recommended.

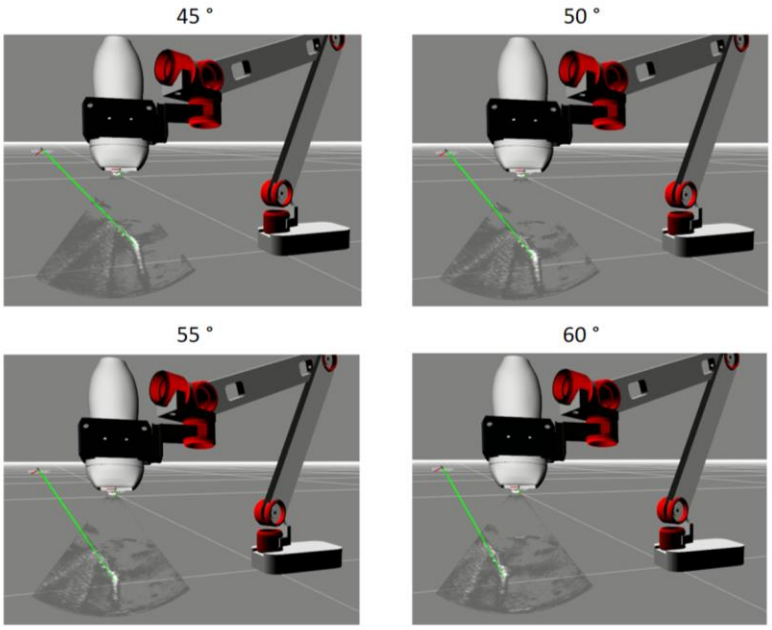

Figure 28. Real-time US scans streamed in RVIZ and overlapped with a green line that indicates the position of the needle for an insertion angle of 45°, 50°, 55° and 60°. The position of the needle's tip is updated with the received linear stage data for insertion depth.

4.4 Ex-vivo and clinical evaluation

4.4.1 Ex-vivo imaging

In this Section are presented the results of the reconstruction of one of the vessels present in the pork leg used for the ex-vivo experiment. Figure 29A and Figure 29B present the reconstructed vessel from 16 segmented US scans before detecting the bifurcation. Later, the previously segmented 16 scans were updated with the other bifurcated vessel, when present, and one more scan including the exact bifurcation point was also segmented. The result of that reconstruction can be observed in Figure 29C and Figure 29D. An alpha value of 0.2 was used for all the reconstructions of the pig vessel. In Figure 29B and Figure 29D is possible to observe with dark red dots the points used for the reconstruction of the shape.

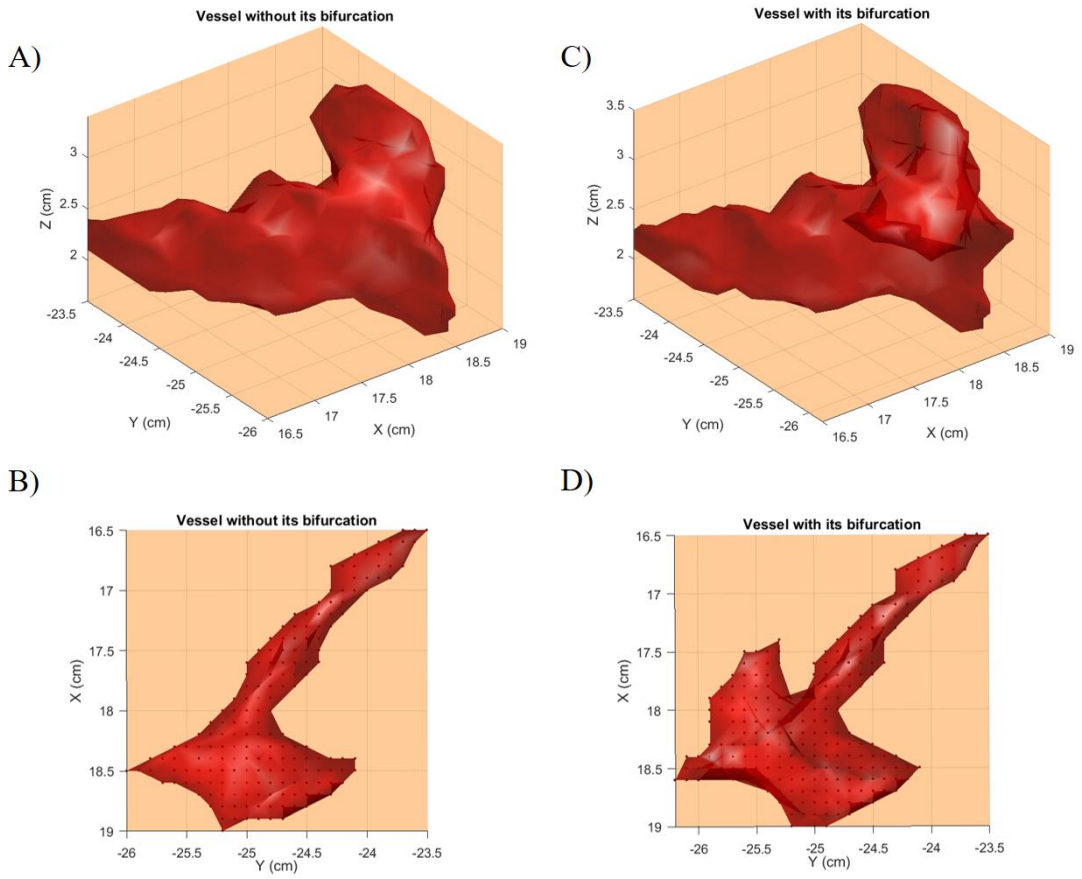

Figure 29. Reconstructed vessel from a pork leg. A) 3D view of the vessels without its bifurcation. B) Visualization of the vessel in A) in the XY plane. C) 3D view of the reconstructed vessel with its bifurcation. D) Visualization of the vessel in C) in the XY plane. In B) and D) are indicated with dark red dots the points used for the reconstruction of the vessel with the alpha-shapes algorithm.

4.4.2 Clinical imaging

The results from the clinical experiment are shown in this section. The vessel that appeared along the whole recording from subject 1 was segmented from in total 22 scans and Figure 30 shows the result of the reconstruction. Furthermore, with dark red points are indicated the points belonging to the segmented scans and used for the creation of the alpha-shape. The alpha-value used in this case was equal to 0.9. In the end, it was possible to reconstruct almost 15 cm of the vessel.

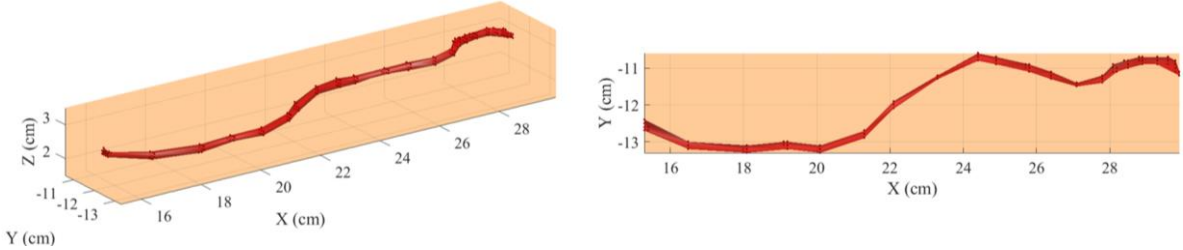

Figure 30. Reconstruction of a vessel of subject 1. Dark red points indicate the points obtained from the segmented scans and used for the reconstruction with the alpha-shapes algorithm.

In the case of subject 2, two vessels were visible along the whole recording. They were segmented from 16 scans whose 3D position is indicated in Figure 31 with dark blue and dark green dots. Figure 30 also shows the reconstruction obtained through the alpha-shapes algorithm with an alpha value of 0.6. Almost 10 cm of the vessels were reconstructed but the reconstruction present some rippling that may indicate a not good performance of the tracking system in this case.

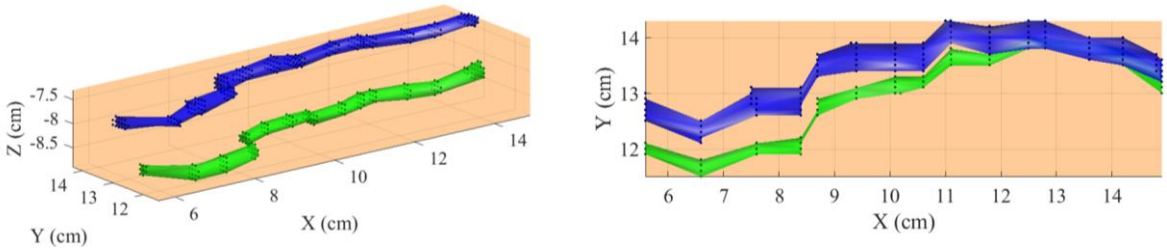

Figure 31. Reconstruction of two vessels of subject 2. Dark blue and green points indicate the points obtained from the segmented scans and used for the reconstruction with the alpha-shapes algorithm.

5. Discussion

After the presentation of the results achieved in this master thesis, this chapter includes in Section 5.1 a summary and discussion of them. The limitations of this study are described in Section 5.2 together with insights about future recommendations. Finally, Section 5.3 highlights the clinical relevance of the thesis research.

5.1 Summary and discussion of results

The non-actuated robotic arm used in this thesis work is just a sensing device that provides the position and orientation coordinates of the probe holder at any moment. Making a non-actuated arm was strategically decided since it is not really necessary for the end goal of the project and it also makes the arm cheaper, lighter and more portable. It is expected that these three factors contribute to the possibility of the arm to reach a wider market and at the same time provide more comfort to the end-user. The arm is more comfortable than an automated handheld assembly but less comfortable than a matrix probe. However, it will be cheaper than a matrix probe and overcomes the limited FOV and the low contrast image limitations of the matrix probes, seen that as a good trade off between price, comfort and outcomes and in favor to the robotic arm.

The first research question of the thesis consisted of finding a clinical application for the robotic arm tracking system through a decision-making process backed with an extensive literature study and interviews with experts. The process led to the decision to first investigate the suitability of the robotic arm tracking system in a liver imaging and biopsy guidance scenario. Multiple factors aimed at this decision. Firstly, the possibility of combining the robotic arm tracking system with a needle holder was considered as highly promising due to the current tendency of combining at the same place and moment organ scanning and biopsy procedure when some suspicious structure is observed during imaging. Secondly, it is an application that would benefit from the extended FOV achieved with US stitching and the prevalence of this type of cancer is high [22].

A commercial ultrasound phantom with an egg-shaped object of known size and shape was scanned to check the performance of the system for object reconstruction. The reconstruction algorithm was based in a first global thresholding with a manually selected threshold value equal to 0.5. This approach was followed due to the clear contrast difference between object and background and also because the sonographer could in this case tune the intensity in the scanner to adapt it to a better image. Once that

the pixels with an intensity value higher than the selected threshold were placed in the 3D space as voxels, an algorithm that removes the data belonging to reflections from the bottom or top of the phantom and surrounding shapes was run. When only voxels belonging to the object of interest where present in the 3D reconstruction space, a closing algorithm with a structuring element with the shape of a sphere of 5mm diameter was applied four times. This structuring element was chosen because it was expected to have sphere like holes of an approximate size of 5 mm in diameter. The reconstructed object matched in shape the object indicated in the datasheet of the phantom and it had a volume of 20.3±0.5 ml while the indicated volume in the datasheet is 21.0 ml. These results demonstrate a good performance of the robotic arm tracking system for object reconstruction due to a reconstruction error smaller than 1 ml. However, the acquisition and processing time with this approach was high.

In the next step, a phantom with a dinosaur shape (complex shape) and two phantoms mimicking lesions with vessels around were made. The objective was to develop an automatic or semi-automatic segmentation and reconstruction algorithm that ideally executes in real-time or that requires a small processing time. It was attempted to achieve that from different approaches involving the use of median filtering as a preprocessing step. Segmenting the area of interest was attempted by applying global thresholding, Otsu's thresholding, the Canny edge detection algorithm and the active contours algorithm together with some morphological openings and closings when needed. However, these approaches only worked for some of the acquired frames and not for all of them due to the not uniform speckle texture of the objects of interest and the generated artifacts from undesired elements such as bubbles or the small fragments of gelatin created after the removal of the copper tubes. These gelatin fragments were vibrating while interacting with the US waves and caused the appearance of ringing artifacts at the edges of the mimicked vessels as it can be seen in Figure 12 and Figure 14. It was then decided to not try further to develop this type of algorithm in a phantom based scenario since it was going to be highly phantom specific.

The final chosen reconstruction approach consists of manually segmenting the objects of interest, labeling each object and applying the alpha-shapes algorithm for their reconstruction. The volume of the egg-shaped object obtained from this approach was equal to 22.1 ml.

However, the volumes of the lesions reconstructed from the mimicking phantoms when one every ten frames were segmented presented overestimation. This can be due to the difficulty in determining the edges of the lesion (Figure 12 as an example) since those were not that clear as in the commercial phantom with the egg-shaped object (Figure 10B). In the lesions made with aluminium oxide particles the difficulty in defining the edges was due to a contrast gradient created along the whole lesions caused by the precipitation of the particles. In the phantom made with Metamucil the reason was a small contrast difference between lesions and parenchyma tissue because of a too low Metamucil concentration difference between both. This small concentration difference was because the lesions mixture started to become thick and that was going to lead to the generation of bubbles while aspiring and expulsing the mixture with the syringe inside of the balloons. Other source of overestimation could be the possible presence of an edge enhancement algorithm involved in the post-processing done by the US scanner or a difference between the real and assumed speed of sound in the phantoms. Furthermore, the resolution of the used US transducer and the assumptions done by the alpha-shapes algorithm could be other sources that affect the volume estimation accuracy in both cases, the commercial phantom and the tissue mimicking phantoms. Also here, another source of overestimation was the assumed voxel size. The estimated volume of lesion 3 in the phantom with Metamucil was 34.3 ml in one of the recordings with the 1 mm^3 voxel size and with a voxel size equal to the scaling factor of the scans was 33.0 ml while the actual volume of the lesion was 30 ml.

Segmenting one every ten frames is a time consuming approach and it was only to obtain an empirical estimation of the phantom, considered close to the ground truth, and used for comparison with the results when less frames are segmented. In this case, it was decided to segment 4 frames of each lesion including the beginning, middle and end of the lesion together with a transverse plane of it. The estimated volumes from this approach were always smaller than the ones obtained in the empirical estimation. This was due to the applied triangulation that missed in the reconstruction the existing curvature in the objects as it can be seen in Figure 25 and Figure 26. However, for the purpose of this project we are mostly interested in the 3D coordinates of the centroid's lesions, point towards which the biopsy needle will be directed. The 3D coordinates of the lesions' centroid of the phantom made with Metamucil could be estimated with a repeatability of less than 1 mm across repeated phantom scans for 72% of centroid coordinates. When comparing the estimated lesions' centroid coordinates in both phantoms obtained through the empirical approach and by segmenting 4 frames per lesion, a difference smaller than 1 mm was observed for 60% of the centroid coordinates and a maximum difference of 4 mm was observed for one of the lesions' centroid coordinates.

Once that the lesion's centroid was calculated, it was possible to find all the paths that connect the centroid with a point at the top of the phantom. It was demonstrated the possibility of evaluating all of these paths and selecting only the ones that would not result in a vessel damage. Furthermore, it was also possible to indicate the shortest needle path with which the fewest amount of tissue would be punctured.

The probe holder was attached to a needle holder in the last step towards illustrating the potential of the robotic arm for biopsy guidance. The attachment ensured that the needle will be always in plane with the probe and thus, the needle will be visible in the acquired US scans. The needle holder incorporated a linear stage that provided real-time data about the insertion depth of the needle. This data together with the definition of a transform that links the probe holder to the needle holder was used to clearly visualize in RViz the updated position of the needle and its tip with a line marker. The indicated needle's position by the marker was overlapped with real-time US data also streamed in RViz for 4 different insertion angles, 45°, 50°, 55° and 60°. A good visual correspondence for the four angles was observed but an accuracy quantification is recommended.

In the last part of the project, the robotic arm tracking system was tested through an ex-vivo and clinical evaluation. The objective was to track and reconstruct vessels to explore how this would be while reconstructing the liver vessels or in future stages, when exploring other clinical applications of the arm as carotid artery imaging. A pork leg was used for the ex-vivo study but it was only possible to reconstruct a small part of the vessels since those were collapsed. However, this case illustrated one important benefit of the system. In the first segmentation of the scans, the bifurcation of the studied vessel was not detected. However, the reconstructed shape gave indications that there was a bifurcation occurring and since the data was saved it was possible to go back through it and this time identify the bifurcation. After segmenting also the other bifurcated vessel, it was possible to see a small part of both vessels. This example illustrates the potential of the system for beginner sonographers that do not have than much experience and are thus, less skilled. In the clinical evaluation it was possible to segment vessels to a longer extend. Two subject participated in the study and from subject 1 it was possible to reconstruct one vessel along 15 cm and from subject 2 it was possible to reconstruct two vessels along more than 10 cm. Through this evaluation it was observed that it is more complex to determine the number of frames to segment or/and every how many frames to segment since this depends on the scanned anatomy. Furthermore, tissue compression can lead to vessel displacement and as a result, a misaligned reconstruction will be obtained. Additionally, the probe holder of this vascular probe was not perfectly fixing the position of the probe, which could have induced a not accurate position and

orientation labelling of the scans. This could explain in the case of subject 2 why the two reconstructed vessels present ripples at the same positions.

5.2 Study limitations and future recommendations

The needle holder used in this experiment to prove the suitability of the arm as an US probe tracking system for liver imaging and biopsy needle guidance is actually designed for an anaesthetic needle. As mentioned in Section 3.3.3 this setup was already available at Philips and it was used for this project to demonstrate the possibility of visualizing the needle and its tip moving in real-time in both, the visualization line marker and the US scan. If this holder is adapted for a biopsy needle, the accuracy of the robotic arm tracking system, reconstruction algorithm and needle path planning algorithm could be tested in a phantom where the lesions have a different colour than the colour of the parenchyma tissue. This can be achieved by adding a colourant to the mixture used for the lesion. The phantom could be made following the same procedure indicated in Section 3.3.1. In this case, lesions of volumes smaller than 10 ml could also be made to test the accuracy of the system for lesions of a smaller size. By checking the colour of the obtained sample with the biopsy needle, it would be possible to verify if the sample was indeed taken from the lesion. Furthermore, this could be in the future a training phantom for the physicians before they used the robotic arm tracking system with a patient.

A clear limitation of this experiment was the presence of artifacts in the phantoms that would not be present in a clinical scenario. The development of an automatic or semi-automatic segmentation algorithm is a complicated task and in this case it was considered that, if a segmentation algorithm for these phantoms was achieved, it was going to be highly phantom specific and it may not work over clinical data. Therefore, the acquisition of tracked US scans with the robotic arm from patients is recommended in the next step for the development of an algorithm based on methods found in literature for liver segmentation using US. It could be studied if some of the automatic or semi-automatic segmentation methods proposed in this thesis perform well on clinical images. If these methods do not provide satisfactory results, the development of a deep learning based algorithm is recommended. Furthermore, in a clinical setting, it will be needed to modified the needle path planning approach since physicians do not usually take a biopsy sample exactly from the centre of the tumor because this part is may be necrotic [28]. Although if the physicians are able to direct the needle to the centroid they can also just change slightly the trajectory and take a sample from the surrounding tumor's tissue. Additionally, in a clinical scenario the shortest path might not always the best path since more elements such as the presence of nerves should also be taken into account during the path planning [28].

The current probe holder setup is cumbersome and allows only for a limited degree of movement. It is then recommended to design and make a needle holder that can be attached to the probe holder as an extension. The needle would be again fixed in such a way that is always in plane with the US beam and thus, visible in the US scans always that the insertion angle is not highly steep or that there is not an object in between obstructing the view. The transform in terms of translation and rotation between the holder and the needle will be known and the same approach as illustrated in this work could be followed. The needle holder should also incorporate a linear stage or a rotational encoder that provides real-time data in regards to the insertion depth. Furthermore, it should incorporate an angular stage or a simpler anchoring mechanism that allows fixing the needle at different insertion angles.

Although liver imaging was the first selected application for the robotic arm as an US probe tracking system, it is also recommended to evaluate its suitability for thyroid gland imaging with purposes of glands volume estimation, nodules detection and biopsy guidance. The main difference between this

application and liver imaging is the size of the involved structures. Once that a good performance of the system is demonstrated and proven for liver imaging, it would be possible to scale-down the developed equipment and algorithms to the smaller size of the thyroid glands and the thyroid nodules scenario – compared to the liver and focal lesions- where a higher accuracy degree will be required. From the only diagnostics group shown in Figure 22 there is a potential of using the robotic arm tracking system for all the presented applications but it is recommended to explore carotid artery imaging and cardiac imaging since it is expected that on them it would be possible to provide the biggest improvement in terms of a need for an extended FOV image and with a better image quality. Obtaining a 3D image where all the carotid plaque is visible enables a more accurate estimation of CPV [11][12] since the plaque has an irregular shape and the real extend of the plaque could be missed in 2D scans if some part of the plaque is out of plane [12]. Additionally, US stitching for cardiac purposed would enable for the majority of the patients the acquisition of 3D images where the whole heart anatomy and function would be visible. In the case of stress echocardiography, a higher reproducibility would be provided [17][18]. Furthermore, in studies involving quantitative measurements, a higher accuracy would be achieved by not having to make geometrical assumptions as in the case of measurements done with 2D US scans or 3D US scans obtained with matrix probes where the whole heart anatomy may not fit in only one scan [4]. A challenge will be the development of a gated reconstruction.

5.3 Clinical relevance of the Thesis Research

This research allowed the selection of a clinical application that may highly benefit from ultrasound stitching with the use of a robotic arm probe tracking system. About 70% of radiologists have indicated that directing the needle to the target in percutaneous operations can be complicated by low visibility of the needle [39]. Factors that influence this low visibility are difficulties to align the needle with the US plane, a needle echogenicity below the optimal level and imaging artifacts such as shadowing effects, reverberations and comet tails [39]. Accurate needle placement is crucial during biopsy procedures and that is why a lot of research has been done into this field. Some of the proposed solutions are beam steering, to increase the number of reflections from the needle surface that go back to the transducer, active vibration of the needle during use than can be visualized in colour Doppler mode, or the adaptation of needle surface by applying coating, denting, material scoring or introducing screw patterns [39]. All of these techniques do improve the visibility of the needle but in some cases, this improvement is relatively low and does not provide a solution that is reliable for all use cases.

In this master thesis, a technique that ensures constant in plane imaging of the needle, guaranteeing that the needle is always visible in the image and solving physician's problem of having to manually maintain a constant alignment between the needle and the US plane during the procedure has been provided. Furthermore, the addition of an angular stage or another fixing feature allows the physician to select different insertion angles. This is already provided by some needle guides available in the market and it has been observed that inexperienced users benefit the most from them [40]. The developed method in this research reconstructs the scanned anatomy and shows the possible needle paths that connect the patient's skin and the lesion's centroid and would not result in a vessel damage. It is highly valuable to know the position at which the patient's skin is since the insertion point in the patient's body is already defined. Assuming that the patient does not move and by keeping the base of the robotic arm at the same position, it would be possible to have in the same coordinate system the reconstructed anatomy and the current position of that anatomy. The proposed solution allows for performing a whole biopsy procedure in one go and therefore, the assumption that the patient and the robotic arm do not move in between first scan and retraction is valid. By moving the robotic arm, but not its base, it would be possible to align in the visualization environment the estimated best needle path with the line in the visualization

environment that indicates the exact position of the needle at that moment. Next, the physician can start inserting the needle and the linear stage will provide real-time data about the insertion depth that will update the position of the visualization line. In this way, the physician is provided with a tool where the tip of the needle is perfectly visible. He does not have to make any assumptions from the US images that may lead to failed biopsy samples and the real-time US scans can be used as a confirmation that the position of the tip indicated by the line in the visualization environment does correspond with the real position of the needle's tip. Therefore, the appearance of artifacts in the US image and suboptimal needle echogenicity is not anymore a limitation for the acquisition of a biopsy sample. This provides an easy way to improve the efficiency of the biopsy procedures.

6. Conclusion

Adding spatial tracking to ultrasound probes overcomes some of its limitations such as limited FOV, operator-dependency, surveillance difficulty and low image contrast. US stitching is a method to provide an improvement of those limitations and consists of tracking multiple US scans, label them with their respective position and orientation coordinates and merge them with this information.

Potential clinical applications for a robotic arm have been investigated in this thesis. The robotic arm can be considered as an accessory to the current US scanners and provides a larger degree of freedom compared to automated handled assemblies. The explored applications could be categorized in two main groups, only diagnostics or diagnostic plus interventions. After a literature study and interviews with experts, it was decided that the arm was going to be firstly tested for liver imaging and biopsy guidance. A high potential for the robotic arm was observed into this field due to the need of obtaining extended FOV images of this organ, the high prevalence of liver cancer and the possibility of including a needle holder to the arm to guide the biopsy needle during its trajectory.

By investigating the suitability of this application for the robotic arm tracking system, it was observed that it is possible to reconstruct a scanned volume by manually segmenting some of the scans and applying an alpha-shapes algorithm. The obtained reconstructions were similar in shape to the actual objects but the volumes of the lesions were overestimated in most of the cases by an average percentage error of 14.6%. This could be due to an erroneous operator segmentation of the structures, a different speed of sound in the phantom than the assumed one, a possible post-processing edge enhancement algorithm present in the scanner or due to the applied 3D reconstruction algorithm. A factor that was seen to surely create overestimation of the volumes was the chosen voxel size for the reconstructions but this approach was needed due to computational power limitations.

In spite of this volume overestimation, the most important aspect for the purposes of this research was an accurate estimation of the lesions centroid to which to direct the biopsy needle. A small standard deviation of the centroid coordinates was observed between strategically segmenting 4 frames per lesion, and then decreasing the workload, and segmenting much more scans per lesions. Furthermore, good repeatability between multiple scannings for centroid estimation was observed. The developed method could be a method for phantom reconstruction and centroid estimation but it is recommended to develop in the future an automatic or semi-automatic segmentation algorithm by using clinical data.

Furthermore, it was illustrated how it would be possible to compute all the needle paths that go from the patient's skin to the lesion's centroid without passing a vessel within a specific distance. A key contribution of the research was the demonstration of the benefits of including a needle holder to the robotic arm with a linear stage that indicates the insertion depth. In this way, the needle can be always in plane with the US plane and the physician will not rely only into his expertise to know where the needle tip is in the US image. Now, a line in the visualization environment will clearly show the position of the tip and this position will be updated with the real-time data obtained from the linear stage. Therefore, the real-time US scans could be used just as a confirmation tool to verify the tip's position.

Finally, an ex-vivo and clinical experiment further illustrated the suitability of the robotic arm tracking system in a more clinical scenario. This experiment also showed the importance of having a probe holder that totally fixes the probe in place and possible reconstruction problems than may arise due to tissue compression.

Appendix

Figure 32 and 33 illustrate the results obtained by applying the same algorithm to multiple frames acquired from the phantom with a dinosaur-shaped object. The algorithm consisted in applying a 3x3 median filter, global thresholding with a threshold value equal to 0.2 and two closings with a disc-like structuring element of 5 pixels radius followed by two openings with the same structuring element. Although part of the shape of interest was not segmented in the image shown in Figure 32, due to the not constant texture of the shape, the surrounding artifacts were not included in the final segmented image. Only the reflections at the top of the phantom were included but they could be easily removed by defining that the top pixels should not be taken into account for the reconstruction. Furthermore, it could be possible to include in the final reconstruction the pixels that are not segmented in the image but do belong to the object by acquiring more data at this position and close positions incorporating tilting motions. This could be possible since all the segmented pixels are added up in the reconstruction and the echogenicity of the object from different angles could vary in such a way that for some angles the upper part of the shape would also be segmented with this algorithm. However, Figure 33 shows a case where the algorithm fails not all the surrounding artifacts were removed and those would appear in the reconstruction making more difficult its interpretation and making the reconstruction itself less accurate.

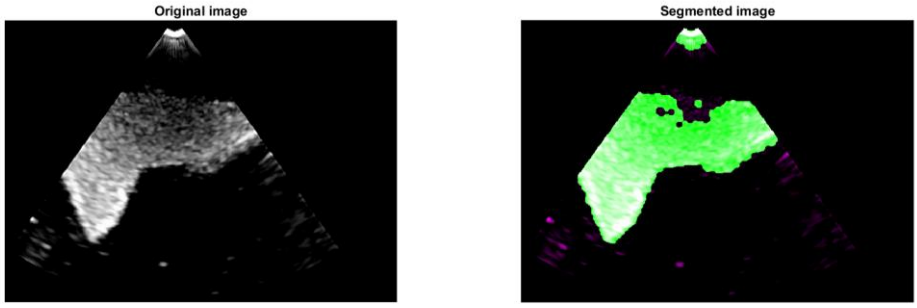

Figure 32. Segmentation achieved by applying a 3x3 median filter, a global thresholding with a threshold value equal to 0.2, two closings with a disc like structuring element of 5 pixels radius and an opening with a disc like structuring element of 5 pixels radius. In the image on the right the original and segmented image are overlapped. In green the result of the segmentation and in purple high intensity pixels that appeared in the original image but not in the segmented image.

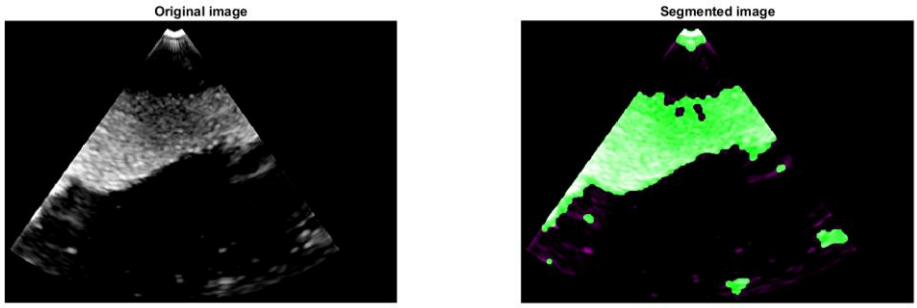

Figure 33. Segmentation achieved by applying a 3x3 median filter, a global thresholding with a threshold value equal to 0.2, two closings with a disc like structuring element of 5 pixels radius and an opening with a disc like structuring element of 5 pixels radius. In the image on the right the original and segmented image are overlapped. In green the result of the segmentation and in purple high intensity pixels that appeared in the original image but not in the segmented image.

Figure 34 and 35 show the results of the multiple stages involved in the segmentation that uses the Canny edge detection algorithm. This segmentation consists of applying a median filter of size 3x3, the Otsu's thresholding method, 2 closings with a disc-like structuring element of 4 pixels, the Canny edge detection algorithm and one dilation to connect the detected borders. The resulting segmented mask is the second biggest area from the detected areas since the biggest area is the background. With the image in Figure 34 a highly accurate segmentation was achieved with this approach but with the image in Figure 35, some reflection artifacts were also segmented. Furthermore, this approach is highly error prone since the assumption that the object of interest will be always the biggest bright object that appears in the scan could not be true in multiple cases.

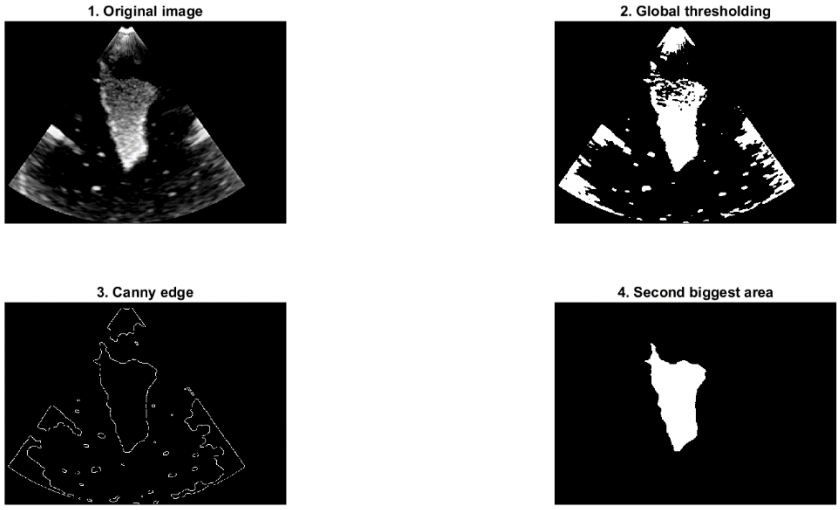

Figure 34. Segmentation obtained by applying a median filter of size 3x3, the Otsu's thresholding method, 2 closings with a disc like structuring element of 4 pixels, the Canny edge detection algorithm and one dilation to connect the detected borders. The resulting segmented mask is the second biggest area of the detected areas.

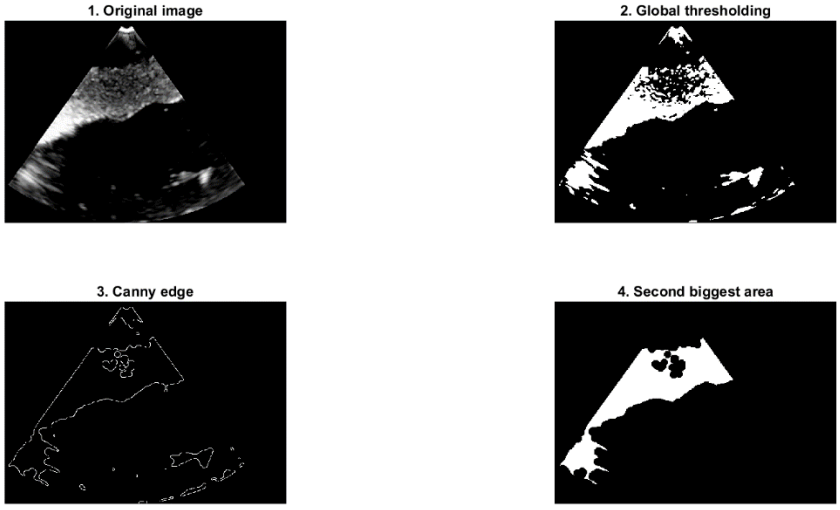

Figure 35. Segmentation obtained by applying a median filter of size 3x3, the Otsu's thresholding mehtod, 2 closings with a disc like structuring element of 4 pixels, the Canny edge detection algorithm and one dilation to connect the detected borders. The resulting segmented mask is the second biggest area of the detected areas.

Figure 36 shows the result of applying a median filter of size 3x3, drawing a rectangle that captures the shape and applying the Chan-Vese algorithm for active contours. In this way, it was intended to develop a semi-automatic segmentation algorithm where the physician should initialize at least the first

rectangular mask that includes the object of interest. In the image on the right, the original and segmented image are overlapped. In green is shown the result of the segmentation and in purple the high intensity pixels that appeared in the original image but not in the segmented image. It is possible to observe that some reflection artifacts were also segmented in this case. It was also possible to appreciate that this algorithm is highly sensitive to the initially selected mask. Slight variations in the selected mask lead to important changes in the segmented area which could make difficult the achievement of robust results following the wanted semi-automatic approach.

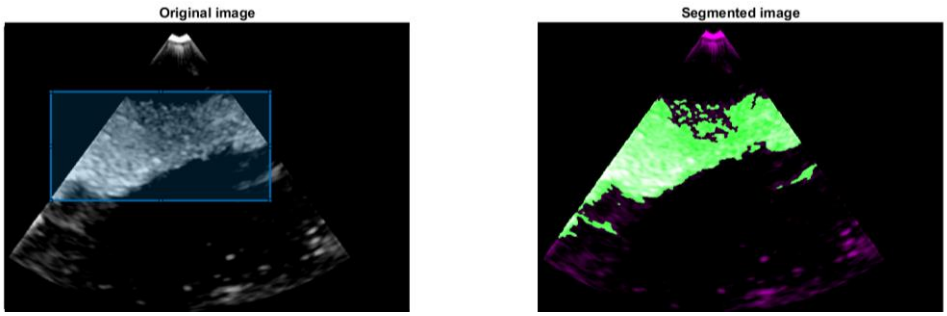

Figure 36. Segmentation obtained by applying a median filter of size 3x3, drawing a rectangle that captures de shape and applying the Chan-Vese algorithm for active contours. In the image on the right, the original and segmented image are overlapped. In green the result of the segmentation and in purple high intensity pixels that appeared in the original image but note in the segmented.

Bibliography

[1] J. M. Prince, J. L. Links, *Medical Imaging Signals and Systems*, Second. PEARSON.

[2] H. Kasban, M. A. M. El-Bendary, and D. H. Salama, "A Comparative Study of Medical Imaging Techniques," *International Journal of Information Science and Intelligent Systems*, vol. 4, no. 2, pp. 37–58, 2015.

[3] Q. Huang and Z. Zeng, "A Review on Real-Time 3D Ultrasound Imaging Technology," *BioMed Research International*, 2017.

[4] A. R. Hareendranathan *et al.*, "Patient Movement Compensation for 3D Echocardiography Fusion," *2016 38th Annu. Int. Conf. IEEE Eng. Med. Biol. Soc.*, pp. 1091–1094, 2016.

[5] E. M. J. Van Disseldorp, J. J. Van Dronkelaar, J. P. W. Pluim, and F. N. Van De Vosse, "Ultrasound Based Wall Stress Analysis of Abdominal Aortic Aneurysms using Multiperspective Imaging," *European Journal of Vascular and Endovascular Surgery*, vol. 59, no. 1, pp. 81–91, 2020.

[6] R. Monfaredi *et al.*, "Robot-assisted ultrasound imaging: Overview and development of a parallel telerobotic system," *Minimally Invasive Therapy & Allied Technologies*, vol. 24, no. 1, pp. 54–62, 2015.

[7] E. M. J. Van Disseldorp, M. H. M. H. Van Den Hoven, F. N. Van De Vosse, R. Marc, H. M. Van Sambeek, and R. G. P. Lopata, "Reproducibility assessment of ultrasound-based aortic stiffness quantification and verification using Bi-axial tensile testing," *Journal Mechanical Behavior of Biomedical Materials*, vol. 103, 2020.

[8] S. K. Rogers, "Evaluation of Tomographic 3D Ultrasound in Vascular Disease," PhD dissertation, Division of Cardiovascular Science, University of Manchester, 2019.

[9] A. M. Kok *et al.*, "Feasibility of wall stress analysis of abdominal aortic aneurysms using three-dimensional ultrasound," *Journal Vascular Surgery*, vol. 61, no. 5, pp. 1175–1184, 2015.

[10] S. Ball, S. Rogers, K. Kanesalingam, R. Taylor, E. Katsogridakis, and C. Mccollum, "Carotid plaque volume in patients undergoing carotid endarterectomy," *The British Journal of Surgery*, vol. 105, no. 3, pp. 262–269, 2018.

[11] K. Saito and H. Yamagami, "Ultrasound Diagnosis of Carotid Plaques," *Journal Neuroendovascular Therapy*, vol. 12, no. 12, pp. 581–591, 2018.

[12] A. M. Johri, M. F. Hétu, and V. Nambi, "Carotid Plaque or CIMT: What is the Future for Carotid US Imaging?," *Current Cardiovascular Risk Reports*, vol. 8, no. 6, pp. 1–8, 2014.

[13] A. M. Johri *et al.*, "Carotid Ultrasound Maximum Plaque Height-A Sensitive Imaging Biomarker for the Assessment of Significant Coronary Artery Disease," *Echocardiography*, vol. 33, no. 2, pp. 281–289, 2016.

[14] L. E. Mantella *et al.*, "Handheld versus conventional vascular ultrasound for assessing carotid artery plaque," *Int. Journal Cardiology*, vol. 278, pp. 295–299, 2019.

[15] M. A. Janvier, F. Destrempes, G. Soulez, and G. Cloutier, "Validation of a new 3D-US imaging robotic system to detect and quantify lower limb arterial stenoses," *Annu. Int. Conf. IEEE Eng.*

Med. Biol. - Proc., pp. 339–342, 2007.

[16] S. Armstrong, "Echocardiography basics for the nurse in cardiovascular care," *British Journal of Cardiac Nursing*, vol. 13, no. 7, pp. 324–329, 2018.

[17] R. P. Steeds *et al.*, "Stress echocardiography in coronary artery disease: A practical guideline from the British Society of Echocardiography," *Echo Research and Practice*, vol. 6, no. 2, pp. G17–G33, 2019.

[18] A. Bouwman, private communication, Jan. 2020.

[19] K. Punithakumar *et al.*, "Multiview 3-D Echocardiography Fusion with Breath-Hold Position Tracking Using an Optical Tracking System," *Ultrasound in Medicine and Biology*, vol. 42, no. 8, pp. 1998–2009, 2016.

[20] K. Punithakumar *et al.*, "Multiview Echocardiography Fusion using an Electromagnetic Tracking System," *2016 38th Annu. Int. Conf. IEEE Eng. Med. Biol. Soc.*, pp. 1078–1081, 2016.

[21] K. Punithakumar *et al.*, "Multiview Three-Dimensional Echocardiography Image Fusion Using a Passive Measurement Arm," *in 40th Annual International Conference of the IEEE Engineering in Medicine and Biology Society*, pp. 903–906, 2018.

[22] H. Neshat, D. W. Cool, K. Barker, L. Gardi, and A. Fenster, "A 3D ultrasound scanning system for image guided liver interventions," *Medical Physiscs*, vol.40, 2013.

[23] V. Blank, J. Wiegand, V. Keim, and T. K. Id, "Evaluation of a novel tomographic ultrasound device for abdominal examinations," *PLoS ONE*, vol.14, no. 6, pp. 1–13, 2019.

[24] P. Poudel, A. Illanes, C. Arens, C. Hansen, and M. Friebe, "Active contours extension and similarity indicators for improved 3D segmentation of thyroid ultrasound images," Proc. SPIE 10138, *Med. Imaging 2017 Imaging Informatics Heal. Res. Appl.*, March 2017.

[25] M. Freesmeyer, L. Knichel, C. Kühnel, and T. Winkens, "Stitching of sensor-navigated 3D ultrasound datasets for the determination of large thyroid volumes – a phantom study," *Medical Ultrasonography*, vol. 20, no. 4, pp. 480–486, 2018.

[26] P. Seifert, T. Winkens, L. Knichel, C. Kühnel, and M. Freesmeyer, "Stitching of 3D ultrasound datasets for the determination of large thyroid volumes – phantom study part II : mechanically-swept probes," *Medical Ultrasonograpphy*, vol. 21, no. 4, pp. 389–398, 2019.

[27] C. K. Jung, J. H. Baek, D. G. Na, Y. L. Oh, K. H. Yi, and H. Kang, "2019 Practice guidelines for thyroid core needle biopsy : a report of the Clinical Practice Guidelines Development Committee of the Korean Thyroid Association," *Journal of Pathology and Translational Medicine*, vol.54, no. 1, pp. 64–86, 2020.

[28] B. Drazenko, private communication, Jan. 2020.

[29] E. Ross, "Freehand three dimensional ultrasound for imaging components of the musculoskeletal system," PhD dissertation, The University of Edinburgh, 2010.

[30] Lucasw, "RVIZ Textured Quads", [Online]. Available: https://github.com/lucasw/rviz_textured_quads, [Accessed October 2019].

[31] R. O. Bude and R. S. Adler, "An easily made, low-cost, tissue-like ultrasound phantom material," *Journal Clinical Ultrasound*, vol. 23, no. 4, pp. 271–273, 1995.

[32] C. Richardson, S. Bernard, and V. A. Dinh, "A cost-effective, gelatin-based phantom model for learning ultrasound-guided fine-needle aspiration procedures of the head and neck," *Journal Ultrasound in Medicine*, vol. 34, no. 8, pp. 1479–1484, 2015.

[33] H. Morehouse, H. P. Thaker, and C. Persaud, “Addition of Metamucil to Gelatin for a Realistic Breast Biopsy Phantom,” *Journal Ultrasound Medicine*., vol. 26, no. 8, pp. 1123–1126, 2007.

[34] G. Hocking, S. Hebard, C. H. Mitchell, and Þ. Fanzca, “A Review of the Benefits and Pitfalls of Phantoms in Ultrasound-Guided Regional Anesthesia,” *Regional Anesthesia Pain Medicine*, vol. 36, no. 2, pp. 162–170, 2011.

[35] J. D. Gardiner, J. Behnsen, and C. A. Brassey, “Alpha shapes : determining 3D shape complexity across morphologically diverse structures,” *BMC Evolutionary Biology*, vol. 18, no. 1, pp. 1–16, 2018.

[36] A. Subasinghe and C. De Alwis, “A review on ultrasound image pre-processing, segmentation and compression for enhanced image storage and transmission,” *KDU International Research. Conference KDUIRC*, no. 09, pp. 106–112, 2018.

[37] S. Das, J. Saikia, S. Das, N. Goni, and S. Engineer, “A COMPARATIVE STUDY OF DIFFERENT NOISE FILTERING,” 2015.

[38] E. M. J. Van Disseldorp, private communication, Jan. 2020.

[39] N. J. van de Berg, J. A. Sánchez-Margallo, A. P. van Dijke, T. Langø, and J. J. van den Dobbelsteen, “A Methodical Quantification of Needle Visibility and Echogenicity in Ultrasound Images,” *Ultrasound in Medicine and Biology*, vol. 45, no. 4, pp. 998–1009, 2019.

[40] H. J. Scholten, A. Pourtaherian, N. Mihajlovic, H. H. M. Korsten, and R. A. Bouwman, “Improving needle tip identification during ultrasound-guided procedures in anaesthetic practice,” *Anaesthesia*, vol. 72, no. 7, pp. 889–904, 2017.